

NASA Technical Paper 1746

NASA
TP
1746
c. 1

LOAN COPY: R
AFWL TECHNIC
KIRTLAND AFB

0067664



TECH LIBRARY KAFB, NM

Deconvolution and Analysis of Wide-Angle Longwave Radiation Data From Nimbus 6 Earth Radiation Budget Experiment for the First Year

T. Dale Bess, Richard N. Green,
and G. Louis Smith

DECEMBER 1980

The NASA logo, consisting of the word "NASA" in a bold, italicized, sans-serif font.



NASA Technical Paper 1746

Deconvolution and Analysis of
Wide-Angle Longwave Radiation
Data From Nimbus 6 Earth
Radiation Budget Experiment
for the First Year

T. Dale Bess, Richard N. Green,
and G. Louis Smith
*Langley Research Center
Hampton, Virginia*

NASA

National Aeronautics
and Space Administration

**Scientific and Technical
Information Branch**

1980

SUMMARY

One year of longwave radiation data from July 1975 through June 1976 from the Nimbus 6 satellite Earth radiation budget experiment is analyzed by representing the longwave radiation field by a spherical harmonic expansion. The data are from the wide-field-of-view instrument. Results show that the limit of the spherical harmonic representation is 12th degree, based on degree variance plots from 12 months. Degree variance plots also show that most of the power is in the lower degree terms. The axisymmetric (zonal) terms dominate, with their coefficients representing approximately 80 percent of the degree variance. Contour maps of the radiation field for 12 months show the geographical distribution of Earth emitted radiant exitance ($W\cdot m^{-2}$) and reveal areas of high and low emitted radiation. The analysis also shows differences in the Earth emitted radiation between the Northern and Southern Hemispheres, presumably due to land and ocean distributional differences.

INTRODUCTION

The nonuniform distribution of radiative heating and cooling over the Earth drives the motion of the atmosphere and oceans, and an understanding of the interaction between the radiation and the dynamics of the atmosphere and oceans is required for understanding climate processes. For this reason, several Earth radiation instruments of increasing sophistication have flown on spacecraft. As early as 1960, instruments for measuring the Earth's radiation budget were flown on Explorer 7 (Vonder Haar (1968)). Since then, a number of satellites have made Earth radiation budget measurements. The ESSA meteorological satellites, the Nimbus satellites, NOAA 1, and ITOS 1 are some of the satellites which have made Earth radiation budget measurements. Radiometers flown on these satellites have provided a wealth of Earth radiation budget data, including longwave measurements, shortwave measurements, wide-field-of-view (WFOV) measurements, and scanning radiometer measurements. Descriptions of these satellites, and analysis of data from them, have been reported by numerous authors such as Raschke et al. (1973), Weaver and House (1979), Ellis et al. (1978), and Green and Smith (1978).

The most recent instrument flown on a satellite for making Earth radiation measurements was the Earth radiation budget (ERB) instrument aboard the Nimbus 6 and Nimbus 7 spacecraft (Smith et al. (1977); Jacobowitz et al. (1979)). The ERB instrument includes two Earth viewing WFOV radiometers, one which measures total irradiance (0.2 to 50 μm) and another which measures shortwave (SW) irradiance (0.2 to 3.8 μm). The difference between the two irradiances is the longwave (LW) or Earth emitted radiation. The ERB instrument has been providing WFOV measurements since July 1975. These WFOV data are suitable for studying large-scale processes over large spatial scales. WFOV sensors integrate radiant exitance ($W\cdot m^{-2}$) from all portions of the Earth atmosphere systems within their fields of view. For the Nimbus 6 spacecraft at an altitude of about 1100 km, the field of view is the entire disk of the Earth.

A deconvolution technique (Smith and Green (1976); Green and Smith (1978)) is applied in this paper to enhance the resolution of the WFOV measurements. Deconvolution represents the radiant exitance at the top of the atmosphere (denoted by TOA and defined herein to be at an altitude of 30 km) by a truncated series of spherical harmonics. Much of the earlier work on radiation budget from satellites has used the geometric shape factor technique to give radiant exitance at TOA. The two techniques are equivalent for global average estimates, but deconvolution gives more information at higher orders.

The Nimbus 6 ERB WFOV data have been analyzed by various investigators. Jacobowitz et al. (1979) recently analyzed and published the results of the first 18 months of ERB measurements. The inverse square approximation (geometric shape factor) was used to determine the radiant exitance at TOA. Some of the earlier investigations have concentrated on the data for August 1975. One such analysis, reported by Smith et al. (1977), defined the monthly mean radiation field by a global contour plot and the global mean. The data analysis technique also employed the inverse square approximation. Green and Smith (1978) analyzed the same data using the technique of parameter estimation and the concept of deconvolution. The parameter estimation technique used in the analysis by Green and Smith is based on solving a system of simultaneous measurement equations using least squares.

In the present paper, a deconvolution (resolution enhancement) technique is presented to study the annual cycle of the distribution of the Earth's LW radiation. The study is based on 1 year of WFOV data from July 1975 through June 1976. The resolution enhancement technique was used to analyze the data and extract mean radiation fields on a monthly basis. However, instead of considering each measurement individually, the data were averaged over 5° by 5° grid areas at satellite altitude. This averaging technique reduced the computational burden at the expense of smoothing the data. This data set was analyzed to produce radiant exitances at TOA. The deconvolution technique takes advantage of the fact that spherical harmonics are the eigenfunctions of the measurement operator and reduces the radiant exitance field from satellite altitude to TOA by dividing by the appropriate eigenvalues.

SYMBOLS

a_n^m, b_n^m	complex coefficients of spherical harmonics for degree n and order m, W^{-m-2}
C_m	integral defined by equation (14)
C_n^m, S_n^m	real coefficients of spherical harmonics at top of atmosphere for degree n and order m, W^{-m-2}
\hat{C}_n^m, \hat{S}_n^m	real coefficients of spherical harmonics at satellite altitude for degree n and order m, W^{-m-2}
$d\sigma$	differential surface element

$g(\alpha)$	angular response function
h	satellite altitude above r_e , 1070 km
I_n^m	integral defined by equation (16)
K	total number of global 5° by 5° grids, 1654
k	grid region
k'	reflection about equator of k th grid region
L	radiance, $W\text{-m}^{-2}\text{-sr}^{-1}$
\mathcal{L}	linear integral measurement operator defined in equation (4)
M	radiant exitance at top of atmosphere, $W\text{-m}^{-2}$
m	measurement, $W\text{-m}^{-2}$
m_k	average of measurements in k th grid region, $W\text{-m}^{-2}$
N	degree of spherical harmonic expansion
N_n^m	normalizing factor for spherical harmonics of degree n and order m
P_n^m	associated Legendre polynomials of degree n and order m
$R(\theta)$	limb-darkening function for emitted radiation
r_e	radius to top of Earth atmosphere system, 6408.165 km
S_m	integral defined by equation (15)
t	time
Y_n^m	complex spherical harmonics of degree n and order m
$\hat{Y}_n^m, \tilde{Y}_n^m$	real spherical harmonics of degree n and order m (see eqs. (9) and (10))
α	cone angle at satellite from nadir to surface element at top of atmosphere, deg
γ	Earth central angle between satellite nadir to a point on surface at top of atmosphere, deg
δ_n^m	Kronecker delta
Θ	colatitude, deg

Θ_s	colatitude of subsatellite point, deg
θ	zenith angle of exiting ray, deg
λ_n	nth eigenvalue of measurement operator
σ_n^2	degree variance for degree n , $W^2\text{-m}^{-4}$
Φ	longitude, deg
Φ_s	longitude of subsatellite point, deg
ϕ	azimuth angle of exiting ray, deg
Ω	solid angle at satellite subtended by surface element, sr

DATA SAMPLE

The Earth radiation budget (ERB) instrument aboard the Nimbus 6 satellite obtained Earth radiation measurements with wide-angle and scanning narrow-angle radiometers. A description of the ERB instrument is given by Smith et al. (1977). Only measurements with the wide-angle radiometers are considered in this paper. The wide-angle radiometer sensed radiation in two channels; one measured total irradiance (0.2 to 50 μm), the other, shortwave irradiance (0.2 to 3.8 μm). Twelve months of these measurements, beginning July 2, 1975, and ending June 29, 1976, were supplied on magnetic tapes by the National Oceanic and Atmospheric Administration (NOAA). Only the longwave radiation component is analyzed herein, and this component was obtained by subtracting the measured shortwave component from the measured value of total irradiance. All measurements from the data tapes are at satellite altitude; and in the analysis which follows, all measurements are increased by 11 percent as a calibration correction. This correction is discussed by Smith et al. (1977) and accounts for a discrepancy between the ERB experiment fixed wide-angle measurements and the integration of scanning narrow-angle measurements.

For most of the data period (July 2, 1975, to June 29, 1976) the ERB instrument operated on a nominal duty cycle of 2 days on and 2 days off; however, because of operational considerations, this schedule was not rigorously followed. Measurements were taken at 4-second intervals during the time the instrument was operating. However, the data tapes supplied by NOAA and on which the analysis in this paper is based reduced the amount of data by averaging every four measurements. This caused some smoothing and gave irradiance measurements at 16-second intervals. Figure 1 is a 12-month calendar showing the approximate time periods covered by the data set as received from NOAA. Each day on the calendar begins at 12 midnight, and the dark bands represent the approximate time periods during which data were recorded.

DATA EDITING

Some measurements were edited from the data set because near sunrise and sunset the WFOV sensor was exposed to the Sun (Jacobowitz et al. (1979)). Exposure to the Sun was due to the design of the wide-angle radiometer. In order for the wide-angle radiometer to view the entire Earth disk, the actual field of view is about 8° larger than the Earth disk and includes a thin annulus of deep space. When the satellite is near sunrise or sunset, the Sun comes into view and contaminates the measurements. When the Sun is on the horizon at sunrise and sunset, the Sun zenith angle at the subsatellite point is 121.5° . This is shown in figure 2. Allowing for a 2° margin on each side of the thin annulus resulted in a range of Sun zenith angles from 111.5° to 123.5° . Based on plots of SW and LW measurements near sunrise and sunset for a few orbits during the month of August 1975, deleting measurements when the Sun zenith angle ranges from 111.5° to 123.5° is sufficient for eliminating Sun contaminated measurements.

The Sun contaminated measurements introduce an additional sampling bias in the Nimbus 6 data. (A bias in the data already exists because the orbit of Nimbus 6 is Sun synchronous, meaning that the radiant exitance at any latitude is based on measurements made only at two local times.) Since the Sun contaminated measurements occur at night (Sun zenith $> 90^\circ$), the editing out of these data reduces the number of samples at night while leaving the daytime data set intact. If the day and night measurements are significantly different, then the radiant exitance for the zone in question will be biased toward the daytime values. No attempt was made to adjust for this effect.

The zone showing the deficiency in number of measurements depends on the time of year. Figure 3 shows the number of measurements for different zones for the month of September. The maximum deficiency occurs between $\pm(60^\circ$ to $65^\circ)$ latitude. Figure 3 also shows that the least number of measurements occurs in the $\pm(80^\circ$ to $85^\circ)$ zone. The measurements in this zone were all located near $\pm 80^\circ$ since the orbit only goes to about $\pm 80.1^\circ$ latitude. The largest number of measurements occurs in the $\pm(75^\circ$ to $80^\circ)$ zone, and the zones in between are sampled about equally except for the deficiency due to Sun contaminated measurements. The number of zonal measurements is dictated by the inclination of the Sun synchronous orbit of Nimbus 6. The dashed line in figure 3 shows how the number of measurements would change if Sun contaminated measurements were not deleted. Between 6 and 7 percent of the measurements for September were deleted because they were contaminated by the Sun. It should also be noted from figure 3 that when Sun contaminated measurements are not deleted, the number of measurements at about 65° north latitude is less than at 65° south latitude. This data dropout is due to the data acquisition station in Alaska.

A possible source of error in the longwave measurements which could vary from 1 to 4 W-m^{-2} was caused by a thermal transient in the shortwave measurements due to irradiation of the sensor at spacecraft sunset (Green and Smith (1978)). No attempt was made to correct for this transient in the data.

Measurements were also omitted if they were greater than 240 W-m^{-2} or less than 50 W-m^{-2} at satellite altitude. The criterion for keeping measurements between the range 50 and 240 W-m^{-2} was based upon visual inspection of plots showing radiant exitance versus time for all measurements. Another criterion deleted a measurement if its value changed by more than 10 W-m^{-2} from the preceding measurement over a 16-second interval. This criterion is based on the decision to omit measurements with values greater than the 3σ value of the difference of all adjacent measurements, where adjacent measurements are not separated in time by more than 16 seconds. The 3σ value for the 3-month period of July, August, and September is 8 W-m^{-2} .

Parts of the 12-month data set had anomalous measurements even after the preceding editing had been completed. The anomalies were discovered by visually inspecting radiant exitance-time plots of all measurements for each month of the 12-month data period. Figure 4 shows a composite of one of these plots which shows some anomalies in the data. The anomalies are characterized by periods of unusually low, unusually high, and erratic radiant exitance values.

Measurements for a 2-hour period on July 10 and a 2.5-hour period on July 17 were deleted because of erratic spiked data. About 2 days of measurements were deleted between July 21 and July 23 because average values suddenly dropped to about 90 W-m^{-2} . The reason for this sudden decrease in radiant exitance is not known. Another questionable set of data was omitted on August 16, 1975. Starting at 1000 hours GMT, the measurements gradually decreased in value during a full satellite revolution and then stabilized at values approximately 30 W-m^{-2} lower than expected. This problem occurred at the end of a data acquisition period; however, the measurements from the next data period did not exhibit the problem. The reason for the gradual decrease in radiant exitance is not known. Approximately 15 hours of measurements were deleted between September 5 and September 6 because of a sudden increase in radiant exitance. Measurements were deleted from October 23 through October 31 because of operational problems. The net effect was incorrect radiant exitance averages for some grid regions. About 3 hours of data in January 1976 were edited out because of anomalous measurements on January 12. Sixteen hours of measurements on February 19 and 30 hours of measurements between February 28 and February 29 were edited out. Measurements taken during the first half of March were edited out. The February and March measurements were deleted because of operational problems. Ten hours of measurements on June 14 were edited out because of erratic values of radiant exitance.

After anomalous measurements were deleted from the data, a few questionable points still remained in the data. The following procedure was used in an effort to delete as many of these anomalous measurements as possible. Measurements were grouped into 5° latitudinal bands. Any measurement within a band that differed by more than 2σ from the average radiant exitance in that band was edited out. This editing procedure caused about 4 percent of the measurements to be deleted.

The total number of measurements for the 12-month period, on which the analysis in this paper is based, was about 588 000 after all editing. This

figure represents about 30 percent of the maximum number of measurements for the year had the ERB instrument made measurements at 16-second intervals uninterrupted.

ANALYSIS TECHNIQUE

The ERB wide-angle data were used to estimate the longwave radiative field at the top of the atmosphere (defined herein as 30 km). The radiative field was represented by a spherical harmonic expansion, and the coefficients were estimated with measurement data.

Measurement Model

The top of the Earth atmosphere system was approximated by a sphere of radius r_e . The emitted radiance L leaving any point E on this surface is, in general, a function of colatitude Θ , longitude Φ , zenith angle θ , azimuth angle ϕ , and time t . (See fig. 5.) Thus, the measurement m at satellite altitude h , colatitude Θ_s , and longitude Φ_s is given by

$$m(\Theta_s, \Phi_s, t) = \int_{\text{FOV}} L(\Theta, \Phi, \theta, \phi, t) g(\alpha) d\Omega \quad (1)$$

where Ω is the differential of solid angle at the satellite subtended by the surface element, α is the cone angle at the satellite from the local vertical to the surface element, and the integration is over the field of view (FOV) of the sensor (Green and Smith (1978)). The function $g(\alpha)$ is the angular response of the sensor to incoming radiation and, for the ERB fixed wide-angle radiometer, has been modeled as a perfectly black flat-plate sensor, or

$$g(\alpha) = \cos \alpha \quad (2)$$

Also, the radiance field was modeled as being independent of ϕ ; that is,

$$L(\Theta, \Phi, \theta, t) = \frac{1}{\pi} M(\Theta, \Phi, t) R(\theta) \quad (3)$$

where M is the radiant exitance at the top of the atmosphere and $R(\theta)$ is a directional function assumed to be independent of position and dependent only upon the zenith angle of the exiting ray. The time dependence is removed by considering monthly averages of measurements. Substituting equations (2) and (3) into equation (1) yields

$$m(\Theta_S, \Phi_S) = \frac{1}{\pi} \int_{\text{FOV}} M(\Theta, \Phi) R(\theta) \cos \alpha \, d\Omega \quad (4)$$

or

$$m(\Theta_S, \Phi_S) = \mathcal{L}[M(\Theta, \Phi)]$$

where \mathcal{L} denotes the linear integral measurement operator of equation (4). It has been shown by Smith and Green (1976) that the eigenfunctions of this linear operator are spherical harmonics for any $R(\theta)$; that is,

$$\mathcal{L}[Y_n^m](\Theta_S, \Phi_S) = \lambda_n Y_n^m(\Theta_S, \Phi_S) \quad (5)$$

where $Y_n^m(\Theta_S, \Phi_S)$ is a spherical harmonic of order m and degree n evaluated at the subsatellite point. The associated eigenvalue λ_n is given by

$$\lambda_n = 2 \int_{\alpha=0}^{\alpha=\alpha_h} P_n^0(\cos \gamma) R(\theta) \cos \alpha \sin \alpha \, d\alpha \quad (6)$$

where $P_n^0(\cos \gamma)$ denotes the Legendre polynomial of degree n as a function of the Earth central angle γ . (See fig. 5.) The integration is from nadir ($\alpha = 0$) to α_h , where α_h is the cone angle to the horizon. Eigenvalues through degree 12 are listed in table I for both a Lambertian and limb-darkening model (Raschke et al. (1973); Green and Smith (1978)).

Over most of the region subtended by the Nimbus 6 WFOV radiometer, $g(\alpha)$ has a $\cos \alpha$ response except for an enhanced response near 60° which is thought to be due to multiple reflections from the ERB instrument. However, since the amount of energy contributed to the measurements from 60° is small, it is felt that modeling the radiometer as a cosine response is adequate.

The effect of choosing one directional function for the entire globe has been investigated. An extreme case was considered where the entire globe was assumed Lambertian, then the entire globe was assumed greatly limb-darkened and the two results were compared. The results reflect the sensitivity of $R(\theta)$ being independent of position. The two solutions gave identical global means. The area-weighted mean of the absolute zonal difference of the Lambertian solution and the limb-darkened solution was 0.55 W-m^{-2} . The area-weighted mean of the absolute 10° regional difference of the Lambertian solution and the limb-darkened solution was 0.75 W-m^{-2} . The directional function used in the present study (Green and Smith (1978)) is intermediate to the two directional functions discussed above and is considered to yield good results.

Deconvolution

Because spherical harmonics are eigenfunctions of the measurement operator, it is convenient to represent the radiant exitance at TOA by a truncated series of spherical harmonics; that is,

$$M(\Theta, \Phi) = \sum_{n=0}^N \sum_{m=-n}^n b_n^m Y_n^m(\Theta, \Phi)$$

Also, let the measurements be represented as

$$m(\Theta, \Phi) = \sum_{n=0}^N \sum_{m=-n}^n a_n^m Y_n^m(\Theta, \Phi)$$

and from equations (4) and (5) it follows that

$$M(\Theta, \Phi) = \sum_{n=0}^N \sum_{m=-n}^n \frac{a_n^m}{\lambda_n} Y_n^m(\Theta, \Phi)$$

where a_n^m and b_n^m , in W^{-m-2} , are complex coefficients of spherical harmonics.

Estimation of Coefficients

For the purposes of this analysis, a real formulation of the spherical harmonics was used. Thus, the radiant exitance at the top of the atmosphere is

$$M(\Theta, \Phi) = \sum_{n=0}^N \sum_{m=0}^n \lambda_n^{-1} \left[\hat{C}_n^m \hat{Y}_n^m(\Theta, \Phi) + \hat{S}_n^m \tilde{Y}_n^m(\Theta, \Phi) \right] \quad (7)$$

where \hat{C}_n^m and \hat{S}_n^m are real coefficients and are estimated from the measurements such that

$$m(\Theta, \Phi) = \sum_{n=0}^{\infty} \sum_{m=0}^n \left[\hat{C}_n^m \hat{Y}_n^m(\Theta, \Phi) + \hat{S}_n^m \tilde{Y}_n^m(\Theta, \Phi) \right] \quad (8)$$

Moreover, the following definitions apply:

$$\hat{Y}_n^m(\Theta, \Phi) = N_n^m \cos(m\Phi) P_n^m(\cos \Theta) \quad (9)$$

$$\tilde{Y}_n^m(\Theta, \Phi) = N_n^m \sin(m\Phi) P_n^m(\cos \Theta) \quad (10)$$

$$N_n^m = \left[(2n+1)(n-m)! \frac{(2-\delta_0^m)}{(n+m)!} \right]^{1/2} \quad (11)$$

$$\int_{\text{Sphere}} \hat{Y}_n^m \hat{Y}_h^k d\sigma = \int_{\text{Sphere}} \tilde{Y}_n^m \tilde{Y}_h^k d\sigma = 4\pi \delta_n^h \delta_m^k \quad (12)$$

$$\int_{\text{Sphere}} \hat{Y}_n^m \tilde{Y}_h^k d\sigma = 0 \quad (13)$$

Also, the following notation will be convenient:

$$C_m(\Phi_1, \Phi_2) = \int_{\Phi=\Phi_1}^{\Phi=\Phi_2} \cos(m\Phi) d\Phi \quad (14)$$

$$S_m(\Phi_1, \Phi_2) = \int_{\Phi=\Phi_1}^{\Phi=\Phi_2} \sin(m\Phi) d\Phi \quad (15)$$

$$I_n^m(\Theta_1, \Theta_2) = \int_{\Theta=\Theta_1}^{\Theta=\Theta_2} P_n^m(\cos \Theta) \sin \Theta d\Theta \quad (16)$$

Multiplying equation (8) by $\hat{Y}_n^m(\Theta, \Phi)$ and integrating over the sphere, taking into account the orthogonal conditions of equations (12) and (13), gives the coefficients at satellite altitude as a function of the measurements; that is,

$$\hat{C}_n^m = (4\pi)^{-1} \int_{\text{Sphere}} m(\Theta, \Phi) \hat{Y}_n^m(\Theta, \Phi) d\sigma \quad (17)$$

However, the measurements $m(\Theta, \Phi)$ are not known everywhere but only at discrete points, so that equation (17) cannot be applied directly. This problem was overcome by dividing the sphere into grid regions and assuming $m(\Theta, \Phi)$ was constant over each region. Thus, m_k denotes the average of all measurements that are in the k th region. The coefficients in equation (17) are given by

$$\hat{C}_n^m = (4\pi)^{-1} \sum_{k=1}^K m_k \int_{\text{Region } k} \hat{Y}_n^m(\Theta, \Phi) d\sigma$$

and from equation (9)

$$\hat{C}_n^m = N_n^m (4\pi)^{-1} \sum_{k=1}^K m_k \int_{\Phi=\Phi_1(k)}^{\Phi=\Phi_2(k)} \cos(m\Phi) d\Phi \int_{\Theta=\Theta_1(k)}^{\Theta=\Theta_2(k)} P_n^m(\cos \Theta) \sin \Theta d\Theta$$

and from equations (14) and (16)

$$\hat{C}_n^m = N_n^m (4\pi)^{-1} \sum_{k=1}^K m_k C_m(k) I_n^m(k) \quad (18)$$

Similarly,

$$\hat{S}_n^m = N_n^m (4\pi)^{-1} \sum_{k=1}^K m_k S_m(k) I_n^m(k) \quad (19)$$

The regions as defined in this analysis are approximately equal area regions, the sides of which are latitude and meridian lines. At the equator the regions are square. For 5° by 5° regions, the sphere is divided into 5° latitudinal bands and each band is divided into an integral number of areas such that each area has approximately the same area. The band from 0° to 5° colatitude contains three regions. The band from 5° to 10° colatitude contains nine regions, etc., down to the band from 85° to 90° colatitude, which contains 72 square regions, 5° by 5°. The total number of regions for a 5° by 5° grid system is $K = 1654$ for the entire globe.

Equations (18) and (19) provide a very efficient way to determine the spherical harmonic coefficients of the measurement representation. First, the total number of measurements is greatly reduced by averaging all measurements in the same region. The integrals C_m and S_m are rapidly computed recur-

sively with the trigonometric addition formulas. Recursive formulas for I_n^m are given in the appendix. The computational effort is halved by taking advantage of the symmetry of the grid system about the equator. If k' corresponds to the region that is the reflection about the equator of the k th region,

then it can be shown that $I_n^m(k') = (-1)^{n+m} I_n^m(k)$. Thus, k in equations (18) and (19) need only range over the regions in the Northern Hemisphere, and

$$\hat{C}_n^m = N_n^m (4\pi)^{-1} \sum_{k=1}^{K/2} \left[m_k C_m(k) I_n^m(k) + m_{k'} C_m(k') I_n^m(k') \right] \quad (20)$$

or

$$\hat{C}_n^m = N_n^m (4\pi)^{-1} \sum_{k=1}^{K/2} \left[m_k + (-1)^{n+m_{m_k}} \right] C_m(k) I_n^m(k)$$

Similarly,

$$\hat{S}_n^m = N_n^m (4\pi)^{-1} \sum_{k=1}^{K/2} \left[m_k + (-1)^{n+m_{m_k}} \right] S_m(k) I_n^m(k) \quad (21)$$

The spherical harmonic coefficients of the measurement representation at satellite altitude are computed using equations (20) and (21). The coefficients for the top of the atmosphere are given by

$$C_n^m = \frac{\hat{C}_n^m}{\lambda_n} \quad (22)$$

and

$$S_n^m = \frac{\hat{S}_n^m}{\lambda_n} \quad (23)$$

where λ_n is the nth eigenvalue from equation (6) based on the limb-darkening function $R(\theta)$. When referring to the time-dependent nature of these coefficients, $C_n^m(t)$ and $S_n^m(t)$ are used.

RESULTS AND DISCUSSION

One year of longwave radiation data from the ERB instrument aboard Nimbus 6 and taken during the period July 1975 through June 1976 has been analyzed to estimate the longwave radiant exitance at the top of the atmosphere (TOA). The radiative field was represented by a spherical harmonic expansion, and the coefficients were estimated with measurement data.

Degree Variance

The spherical harmonic coefficients computed using equations (22) and (23) can be used to define the spatial spectrum of the radiation field in terms of degree variance. From Green and Smith (1978), degree variance for a given degree n at satellite altitude is defined to be

$$\sigma_n^2 = \sum_{m=0}^n \left[(\hat{C}_n^m)^2 + (\hat{S}_n^m)^2 \right]$$

At the top of the atmosphere (TOA), the degree variance for a given degree n is

$$\sigma_n^2 \Big|_{\text{TOA}} = \left(\frac{\sigma_n}{\lambda_n} \right)^2$$

The degree variance for all n is analogous to the amplitude spectrum in ordinary harmonic analysis and gives an indication of the power in each spatial frequency. Degree variance plots for each month as a function of degree n at satellite altitude and at TOA are used to establish the limit in degree to which a spherical harmonic representation of the data can be realized. Figure 6 shows the degree variance plot for the average of the 12-month data set for each degree 1 through 30. The lower curve is the degree variance at satellite altitude, and the upper curve represents the degree variance at TOA. Divergence of the two curves begins at about degree 12.

Figure 7, similar to figure 6, shows the standard deviation of average degree variance over 12 months at the top of the atmosphere for degree 1 to degree 30. During the year there are 12 values of σ_n^2 for each degree n . Standard deviation of average degree variance at satellite altitude is similar to the variation at the top of the atmosphere.

The degree at which the spherical harmonic expansion should be truncated impacts the uncertainty of the radiant exitance contour map solutions. Based on a 12-month data set, figure 6 shows the resolution limit of the spherical harmonic representation to be about 12th degree, with the spectral region of higher frequency components beyond 12th degree produced mainly by noise comprised of variations in the radiation field during the month and measurement errors. Monthly sampling does not appear to affect the 12th degree limit on truncation. This can be seen by considering the LW radiation data for March 1976, for which the time average of radiant exitance covered only the second half of the month because of some operational problems. However, the resolution limit was still 12th degree based on the degree variance plot for March.

Spatial sampling of the data for August 1975 averaged over the month for 5° by 5° grid regions and then for $2\frac{1^\circ}{2}$ by $2\frac{1^\circ}{2}$ grid regions showed that the resolution limit did not change when grid size was changed.

Attempting to represent the radiation field beyond the resolution limit of the sensor leads to incorrect values of radiant exitance at TOA because the noise is being amplified by the eigenvalues λ_n .

To give some idea of how sensitive the solution is to the degree of truncation, the measurements for the month of August 1975 were carried out to a 15th degree expansion and then compared with a 12th degree expansion for August, both for a Lambertian model. Results show no difference in global mean, pole-to-pole gradient, and equator-to-pole gradient. The area-weighted mean of absolute zonal differences of 15th degree minus 12th degree was 0.85 W-m^{-2} . The area-weighted mean of absolute 10° grid regional differences was 3.94 W-m^{-2} .

Spherical Harmonic Coefficients

Spherical harmonic coefficients for 12 months of longwave radiation data were computed using equations (22) and (23) which are based on the monthly mean value of the measurements in each of the 1654 grid regions. Results are for a degree 12 spherical harmonic expansion. For a 12th degree expansion, 169 coefficients are required to specify the radiation field.

For a 12th degree spherical harmonic expansion approximately 80 percent of total degree variance is accounted for by the 12 axisymmetric coefficients C_1^0 to C_{12}^0 . The first five axisymmetric coefficients represent about 70 percent of the summed degree variance. The axisymmetric terms for the 12 months of Nimbus 6 longwave radiation data are listed in table II. Nonaxisymmetric terms through degree 12 and through order 12 for the 12 months are shown in table III. Terms below the indicated staircase are cosine terms C_n^m ; terms above the staircase are sine terms S_n^m . Units of all terms are in W-m^{-2} .

Geographical Distribution of Longwave Radiation

Radiation contour maps for each month are shown in figures 8(a) to 8(l). Figure 9 shows monthly averages of zonal emitted radiant exitance for each of the 12 months. In essence, figure 9 shows a profile of each contour map where radiant exitance has been averaged over longitude at each 5° latitude. The patterns in the maps (figs. 8(a) to 8(l)) are mainly influenced by surface temperature, by the mean cloud cover and cloud height, and by the temperature lapse rate and moisture content of the atmosphere. These maps show the geographical distribution of emitted longwave radiant exitance for the 12-month period and are based on a degree 12 spherical harmonic representation of the

radiation field. It can be seen from the contour maps, from figure 9, and from the table of spherical harmonic coefficients (table II) that the radiation field for each month is zonal in character and especially well marked in the Southern Hemisphere.

The contour maps also define the variation of major features for each month. Centers of high and low radiant exitance show some shifting in position throughout the year. Highs are generally located in the tropical and subtropical regions between -35° latitude and $+35^{\circ}$ latitude. A narrow band of lows in temperate and low latitudes between -10° and $+20^{\circ}$ appears throughout the year. These lows appear over areas with high cyclonic activity. Lows extend to high latitudes in both hemispheres, with the extension being a dominant feature in the Northern Hemisphere. Noteworthy are the lows over Greenland, Siberia, Antarctica, Central Africa, and Southeast Asia, the highs over Northern and Southern Africa, and the high over Australia. The lows over Antarctica show up during each month and are presumably picking up the Antarctica ice cap. Lowest emission throughout the year occurs over Antarctica. This low shows some shifting and variability. Emission over Antarctica is in step with the seasons, increasing from September through March and decreasing during the next 6 months. Greenland, the Beaufort Sea off the coast of Alaska, Siberia, and the Siberian Sea with its thick ice shield show the lowest emission over the Arctic, but not as low as the emission over Antarctica. In terms of temperature, the Arctic is much warmer on the average throughout the year than Antarctica.

Another area of low emission is Southeast Asia during the monsoon summer, when the amount of longwave radiation emitted over Southeast Asia is less than the emitted radiation over Greenland during the same time period. This is due to monsoon clouds being relatively opaque with surfaces that are usually high and cold. During the winter months the emitted radiation over Southeast Asia increases because the winter monsoons bring dry, clear weather for several months.

The low over Central Africa appears during each month and shows very little movement. This low is located in the vicinity of the Congo Basin and the Equatorial rain forests, which are characterized by continuously warm weather and abundant rainfall. During the summer season, highs exist over Northern and Southern Africa in the vicinity of the Sahara and Kalahari Deserts. These highs show some movement with the seasons. There is also a high that appears consistently near the western coast of the Australian desert region. This high shows some movement with the seasons.

The monthly contour maps were shown to have a 12th order spherical harmonic expansion. The sensitivity caused by changing the order of expansion shows up clearly in the contour maps. Green and Smith (1978) analyzed the Nimbus 6 longwave data for August 1975 but only produced a 5th order spherical harmonic expansion. Their contour map for August is qualitatively similar to the August contour map from the present analysis. However, the two maps differ in both location and spatial extent of high and low areas of radiation. In effect, the 5th order expansion for the month of August does not contain as much high frequency information of the radiation field as does the 12th order expansion.

Time Histories of Zonal Coefficients

Examination of the $C_n^m(t)$ and $S_n^m(t)$ presented in table II and table III shows that the axisymmetric terms ($m = 0$) dominate up to $n = 5$ with about 70 percent of the degree variance in the first five zonal coefficients. Some of these coefficients have obvious physical meanings.

Figure 10 shows the yearly cycle of the global average $C_0^0(t)$ of emitted longwave radiation. The plot of $C_0^0(t)$ represented by the square symbols in figure 10 is the only term from the present analysis that can be readily compared with global average values of emitted radiation from Nimbus 6 published by other sources, such as Ellis et al. (1978) and Jacobowitz et al. (1979). In making the comparisons, TOA is at 30 km above the Earth's surface in all cases, and the radiant exitance values are averages of daytime and nighttime measurements. All data sets incorporated a calibration correction referred to by Smith et al. (1977). Both Ellis and Jacobowitz used the inverse square approximation to determine radiant exitance at TOA. All three data sets show the same trend in global average for the year. However, the global average of radiant exitance based on the work by Ellis et al. (1978) is about 4 W-m^{-2} higher (on the average) than the global average of radiant exitance from the present work. From January through June the global average from Jacobowitz et al. (1979) compares very well with the global averages $C_0^0(t)$. Also included in figure 10 is a 29-month data set by Ellis et al. (1978) of global average. This data set is comprised of a number of sources. The trend is very irregular, with unusually high values of global radiant exitance in April and May. Some differences in global averages as reported by the different investigators (fig. 10) may be due to the way data were edited before being analyzed. Calibration corrections may have also been different.

The $C_1^0(t)$ term in figure 11 is a measure of hemispherical or pole-to-pole differences. Its annual cycle is seen to have a nearly perfect sine shape, with a total range between its minimum and maximum values of about 20 W-m^{-2} . It does not oscillate about zero but has a bias of 2.5 W-m^{-2} . If the Earth is symmetric

about the equator, one would expect the C_n^0 terms for odd n values to have time histories which are symmetric about the time axis. Thus, the 2.5 W-m^{-2}

bias in the annual cycle of $C_1^0(t)$ is presumed to be due to land and ocean distributional differences between the Northern and Southern Hemispheres. The

$C_2^0(t)$ term in figure 11 may be considered to be a measure of equator-to-pole gradient. It is seen to have an average value of -25.6 W-m^{-2} , with a small variation.

The $C_n^0(t)$ terms for $n = 3$ to $n = 12$ are shown in figure 12. The C_3^0 term is nearly sinusoidal, with a total variation of 15 W-m^{-2} and a mean of 4 W-m^{-2} . As with C_1^0 , this bias is presumed to be the result of hemispheric

differences of land and ocean distribution. The C_4^0 term has a mean of approximately -7 W-m^{-2} with variation of 5 W-m^{-2} . Its shape is not so sinusoidal as the C_1^0 or C_3^0 histories. The C_5^0 to C_{10}^0 terms each have a significant annual sine component, and the C_6^0 and C_8^0 terms have a bias such that they do not change signs. The maximum absolute value decreases with increasing n until C_{11}^0 and C_{12}^0 , which are small and show little discernible pattern.

Whether the lack of pattern in the computed values of C_{11}^0 and C_{12}^0 is due to the nature of the atmosphere or due to the limitations of sampling and analysis is unclear at present.

Effect of Grid System

The reason for using the grid-system averaging technique is to reduce the computer computational burden. This is done at the expense of smoothing the data. One way to assess the effect of grid systems on the present analysis, which is based on a 5° by 5° grid system, is to compare the degree variance plots based on a different size grid system. This comparison was done for the month of August 1975 for a 5° and a $2\frac{1}{2}^\circ$ grid system. The computational effort is 4 times greater for the $2\frac{1}{2}^\circ$ grid system. The results are shown in figure 13. Out to degree 7, the degree variance plots for the two grid systems are the same. From degree 7 to degree 12, where their contribution is small, the degree variances differ only by a small amount. Thus, based on comparing degree variances, no significant improvement is gained in going from a 5° by 5° grid system to a $2\frac{1}{2}^\circ$ by $2\frac{1}{2}^\circ$ grid system.

CONCLUSIONS AND RECOMMENDATIONS

Based upon the results of the analysis of the first year of data from the Nimbus 6 WFOV radiometer, the following conclusions regarding Earth emitted radiation are drawn:

1. Degree variance plots for 12 months of LW radiation data show that the limit for a spherical harmonic representation of the Nimbus 6 WFOV LW data is 12th degree. The degree variance plots also reveal that most of the power is in the lower degree terms. The axisymmetric (zonal) terms dominate, with their coefficients representing approximately 80 percent of the degree variance for a 12-month period.

(2) Contour maps of the radiation field are computed. These maps show the geographical distribution of Earth emitted radiant exitance for 12 months. The maps reveal distinct highs and lows and their shift with the seasons. Highs are generally located between -35° latitude and $+35^{\circ}$ latitude. A band of lows is located between -10° latitude and $+20^{\circ}$ latitude. Lows extend to high latitudes in both hemispheres, with the extension being a dominant feature in the Northern Hemisphere.

(3) Some of the spherical harmonic coefficients have physical meanings; for example, $C_0^0(t)$ is the global average emitted radiation, $C_1^0(t)$ represents the pole-to-pole gradient, and $C_2^0(t)$ is a measure of the equator-to-pole gradient. Comparison of $C_0^0(t)$ from the present study with the global average of emitted radiation computed by Ellis et al. (J. Geophys. Res., vol. 83, no. C4, Apr. 20, 1978) shows that $C_0^0(t)$ is about 4 W-m^{-2} lower than their global average, although the annual trend is the same. The global average from Jacobowitz et al. (J. Atmos. Sci., vol. 36, no. 3, Mar. 1979) shows better agreement with $C_0^0(t)$. The $C_1^0(t)$ term has a bias of about 2.5 W-m^{-2} , presumably due to distributional differences between land and ocean in the Northern and Southern Hemispheres.

4. Based on comparing degree variances, no significant improvement is gained in going from a 5° by 5° grid system to a $2\frac{1}{2}^{\circ}$ by $2\frac{1}{2}^{\circ}$ grid system. Furthermore, the averaging of data over 5° by 5° regions is a reasonable approach.

Subsequent years of data from the Nimbus 6 ERB are needed in order to establish a longer term average of the annual cycle and to provide a basis for studies of interannual variability. Nonaxisymmetric terms need to be analyzed for annual variation. Longitudinal spectra of emitted radiation as a function of latitude need to be computed in order to gain insight into processes causing a nonaxisymmetric distribution.

Langley Research Center
National Aeronautics and Space Administration
Hampton, VA 23665
October 6, 1980

APPENDIX

INTEGRATION OF ASSOCIATED LEGENDRE POLYNOMIALS

The problem is to determine recursive formulas for I_n^m , where

$$I_n^m(\Theta_1, \Theta_2) \equiv \int_{\Theta=\Theta_1}^{\Theta=\Theta_2} P_n^m(\cos \Theta) \sin \Theta \, d\Theta \quad (A1)$$

where $P_n^m(\cos \Theta)$ is an associated Legendre polynomial of degree n and order m and Θ is colatitude. Recursive formulas for I_n^m are given by Fricke (1978). The purpose of this appendix is to expand the derivation and to express the results in a form compatible with this paper.

Equations (A2) and (A3) are obtained from Korn and Korn (1961) as follows (eq. (A2) is equivalent to eq. (21.8-55) in the reference):

$$(n - m + 1) P_{n+1}^m(\cos \Theta) = (2n + 1) \cos \Theta P_n^m(\cos \Theta) - (n + m) P_{n-1}^m(\cos \Theta) \quad (0 \leq m \leq n - 1) \quad (A2)$$

$$\sin^2 \Theta \frac{d}{d(\cos \Theta)} \left[P_n^m(\cos \Theta) \right] = (n + 1) \cos \Theta P_n^m(\cos \Theta) - (n - m + 1) P_{n+1}^m(\cos \Theta) \quad (0 \leq m \leq n) \quad (A3)$$

Integration of equation (A2) using equation (A1) gives

$$I_{n+1}^m(\Theta_1, \Theta_2) = (2n + 1)(n - m + 1)^{-1} \int_{\Theta_1}^{\Theta_2} P_n^m(\cos \Theta) \cos \Theta \sin \Theta \, d\Theta - (n + m)(n - m + 1)^{-1} I_{n-1}^m(\Theta_1, \Theta_2) \quad (A4)$$

APPENDIX

Integration of equation (A3) gives

$$\int_{\Theta_1}^{\Theta_2} \sin^2 \Theta \frac{d}{d(\cos \Theta)} \left[P_n^m(\cos \Theta) \right] \sin \Theta d\Theta = (n+1) \int_{\Theta_1}^{\Theta_2} P_n^m(\cos \Theta) \sin \Theta \cos \Theta d\Theta - (n-m+1) \int_{\Theta_1}^{\Theta_2} P_{n+1}^m(\cos \Theta) \sin \Theta d\Theta \quad (A5)$$

Integration of the left-hand side of equation (A5) by parts gives

$$(n-1) \int_{\Theta_1}^{\Theta_2} P_n^m(\cos \Theta) \cos \Theta \sin \Theta d\Theta = -\sin^2 \Theta P_n^m(\cos \Theta) \Big|_{\Theta_1}^{\Theta_2} + (n-m+1) I_{n+1}^m(\Theta_1, \Theta_2) \quad (A6)$$

Elimination of the integral between equations (A4) and (A6) and collecting terms gives the desired recursion equation

$$I_{n+1}^m(\Theta_1, \Theta_2) = (n+2)^{-1} (n-m+1)^{-1} \left[(2n+1) \sin^2 \Theta P_n^m(\cos \Theta) \Big|_{\Theta_1}^{\Theta_2} + (n-1)(n+m) I_{n-1}^m(\Theta_1, \Theta_2) \right] \begin{pmatrix} m = 0, 1, 2, \dots \\ n = m+1, m+2, \dots \end{pmatrix} \quad (A7)$$

The recursion equation (A7) for I_{n+1}^m requires two initial values, namely, I_m^m and I_{m+1}^m . Equation (A8) is obtained from Korn and Korn (1961) as follows (eq. (A8) is equivalent to eq. (21.8-54) in the reference):

$$P_m^m(\cos \Theta) = (1)(3)(5) \dots (2m-1) \sin^m \Theta \quad (m = 1, 2, \dots) \quad (A8)$$

and from the definition of I_m^m (eq. (A1)),

$$I_m^m(\Theta_1, \Theta_2) = \int_{\Theta_1}^{\Theta_2} (1)(3)(5) \dots (2m-1) \sin^{m+1} \Theta d\Theta \quad (A9)$$

APPENDIX

By integration,

$$I_m^m(\Theta_1, \Theta_2) = (1)(3)(5) \dots (2m-1) \left[-(m+1)^{-1} \sin^m \Theta \cos \Theta \Big|_{\Theta_1}^{\Theta_2} + m(m+1)^{-1} \int_{\Theta_1}^{\Theta_2} \sin^{m-1} \Theta \, d\Theta \right]$$

Substituting from equations (A8) and (A9) gives

$$I_m^m(\Theta_1, \Theta_2) = -(m+1)^{-1} \cos \Theta P_m^m(\cos \Theta) \Big|_{\Theta_1}^{\Theta_2} + m(2m-1)(2m-3)(m+1)^{-1} I_{m-2}^{m-2}(\Theta_1, \Theta_2) \quad (m = 2, 3, \dots) \quad (A10)$$

Evaluating equation (A3) at $n = m$ gives

$$\sin^2 \Theta \frac{d}{d(\cos \Theta)} [P_m^m(\cos \Theta)] = (m+1) \cos \Theta P_m^m(\cos \Theta) - P_{m+1}^m(\cos \Theta) \quad (A11)$$

Differentiating P_m^m of equation (A8) and simplifying yields the result

$$P_{m+1}^m(\cos \Theta) = (2m+1) \cos \Theta P_m^m(\cos \Theta) \quad (m = 0, 1, \dots) \quad (A12)$$

Thus, equation (A10) can be simplified as

$$I_m^m(\Theta_1, \Theta_2) = -(2m+1)^{-1} (m+1)^{-1} P_{m+1}^m(\cos \Theta) \Big|_{\Theta_1}^{\Theta_2} + m(2m-1)(2m-3)(m+1)^{-1} I_{m-2}^{m-2}(\Theta_1, \Theta_2) \quad (m = 2, 3, \dots) \quad (A13)$$

To start this recursion, the values I_0^0 and I_1^1 are needed, or

$$I_0^0(\Theta_1, \Theta_2) = \int_{\Theta_1}^{\Theta_2} (1) \sin \Theta \, d\Theta = -\cos \Theta \Big|_{\Theta_1}^{\Theta_2} \quad (A14)$$

APPENDIX

$$I_1^1(\Theta_1, \Theta_2) = \int_{\Theta_1}^{\Theta_2} (\sin \Theta) \sin \Theta \, d\Theta = \frac{1}{2} (\Theta - \sin \Theta \cos \Theta) \Big|_{\Theta_1}^{\Theta_2} \quad (A15)$$

Next, an expression for I_{m+1}^m is derived. From equations (A12) and (A8),

$$\int_{\Theta_1}^{\Theta_2} P_{m+1}^m(\cos \Theta) \sin \Theta \, d\Theta = (1)(3)(5) \dots (2m-1)(2m+1) \int_{\Theta_1}^{\Theta_2} \sin^{m+1} \Theta \cos \Theta \, d\Theta$$

or

$$I_{m+1}^m(\Theta_1, \Theta_2) = (1)(3)(5) \dots (2m-1)(2m+1)(m+2)^{-1} \sin^{m+2} \Theta \Big|_{\Theta_1}^{\Theta_2}$$

Simplifying with equation (A8) gives

$$I_{m+1}^m(\Theta_1, \Theta_2) = (m+2)^{-1}(2m+3)^{-1} P_{m+2}^{m+2}(\cos \Theta) \Big|_{\Theta_1}^{\Theta_2} \quad (m = 0, 1, 2, \dots) \quad (A16)$$

Thus, in summary, the five recursive formulas for I_n^m are

$$I_0^0(\Theta_1, \Theta_2) = -\cos \Theta \Big|_{\Theta_1}^{\Theta_2} \quad (A14)$$

$$I_1^1(\Theta_1, \Theta_2) = \frac{1}{2} (\Theta - \sin \Theta \cos \Theta) \Big|_{\Theta_1}^{\Theta_2} \quad (A15)$$

$$I_m^m(\Theta_1, \Theta_2) = -(2m+1)^{-1}(m+1)^{-1} P_{m+1}^m(\cos \Theta) \Big|_{\Theta_1}^{\Theta_2} + m(2m-1)(2m-3)(m+1)^{-1} I_{m-2}^{m-2}(\Theta_1, \Theta_2)$$

$$(m = 2, 3, \dots) \quad (A13)$$

APPENDIX

$$I_{m+1}^m(\Theta_1, \Theta_2) = (m+2)^{-1}(2m+3)^{-1} P_{m+2}^{m+2}(\cos \Theta) \Big|_{\Theta_1}^{\Theta_2} \quad (m = 0, 1, 2, \dots) \quad (A16)$$

$$I_{n+1}^m(\Theta_1, \Theta_2) = (n+2)^{-1}(n-m+1)^{-1} \left[(2n+1) \sin^2 \Theta P_n^m(\cos \Theta) \Big|_{\Theta_1}^{\Theta_2} + (n-1)(n+m) I_{n-1}^m(\Theta_1, \Theta_2) \right]$$

$$\left(\begin{array}{l} m = 0, 1, 2, \dots \\ n = m+1, m+2, \dots \end{array} \right) \quad (A7)$$

REFERENCES

1. Ellis, J. S.; Vonder Haar, T. H.; Levitus, S.; and Oort, A. H.: The Annual Variation in the Global Heat Balance of the Earth. *J. Geophys. Res.*, vol. 83, no. C4, Apr. 20, 1978, pp. 1958-1962.
2. Fricke, Clifford L.: The Phase-Integral Method for Radiative Transfer Problems With Highly-Peaked Phase Functions. *J. Quant. Spectros. & Radiat. Transfer*, vol. 20, no. 5, Nov. 1978, pp. 429-445.
3. Green, Richard N.; and Smith, G. Louis: Parameter Estimation Applied to Nimbus 6 Wide-Angle Longwave Radiation Measurements. NASA TP-1307, 1978.
4. Jacobowitz, H.; Smith, W. L.; Howell, H. B.; Nagle, F. W.; and Hickey, J. R.: The First 18 Months of Planetary Radiation Budget Measurements From the Nimbus 6 ERB Experiment. *J. Atmos. Sci.*, vol. 36, no. 3, Mar. 1979, pp. 501-507.
5. Korn, Granino A.; and Korn, Theresa M.: *Mathematical Handbook for Scientists and Engineers*. McGraw-Hill Book Co., Inc., 1961.
6. Raschke, Ehrhard; Vonder Haar, Thomas H.; Bandeen, William R.; and Pasternak, Musa: The Annual Radiation Balance of the Earth-Atmosphere System During 1969-70 From Nimbus 3 Measurements. *J. Atmos. Sci.*, vol. 30, no. 3, Apr. 1973, pp. 341-364.
7. Smith, W. L.; Hickey, J.; Howell, H. B.; Jacobowitz, H.; Hilleary, D. T.; and Drummond, A. J.: Nimbus-6 Earth Radiation Budget Experiment. *Appl. Opt.*, vol. 16, no. 2, Feb. 1977, pp. 306-318.
8. Smith, G. Louis; and Green, Richard N.: Theoretical Analysis of Wide Field of View Radiometer Measurements of Earth Energy Budget. NASA paper presented at Fifth Annual Remote Sensing of Earth Resources Conference (Tullahoma, Tenn.), Mar. 29-31, 1976.
9. Vonder Haar, Thomas Henry: Variations of the Earth's Radiation Budget. Ph. D. Thesis, Univ. of Wisconsin, 1968.
10. Weaver, William L.; and House, Frederick B.: Analysis of Earth Radiation Budget Data From Unrestricted Broadband Radiometers on the ESSA 7 Satellite. NASA TP-1402, 1979.

TABLE I.- EIGENVALUES OF MEASUREMENT OPERATOR

[$r_e = 6408.165$ km; $h = 1070$ km]

n	λ_n for -	
	Lambertian model	Limb-darkening model
0	0.7343	0.7343
1	.7217	.7232
2	.6975	.7014
3	.6632	.6704
4	.6208	.6317
5	.5726	.5873
6	.5214	.5393
7	.4693	.4899
8	.4185	.4408
9	.3707	.3936
10	.3267	.3494
11	.2874	.3091
12	.2526	.2728

TABLE II.- SPHERICAL HARMONIC (ZONAL) COEFFICIENTS FOR 12 MONTHS OF NIMBUS 6 LONGWAVE RADIANT
EXITANCE ($W\text{-m}^{-2}$) THROUGH 12TH DEGREE AT TOP OF ATMOSPHERE^a

	Jul	Aug	Sep	Oct	Nov	Dec	Jan	Feb	Mar	Apr	May	Jun
C_0^0	235.042	235.663	232.706	230.708	228.412	228.963	229.931	229.285	231.055	230.793	232.395	238.222
C_1^0	12.501	11.287	8.171	4.548	-1.003	-5.662	-7.707	-7.817	-4.067	-.151	5.639	11.439
C_2^0	-21.222	-23.354	-25.455	-27.252	-27.313	-26.577	-26.026	-27.664	-27.348	-26.238	-26.131	-25.549
C_3^0	9.966	12.091	7.212	3.856	-1.040	-3.190	-3.204	-2.172	1.907	5.853	8.656	9.044
C_4^0	-8.960	-9.304	-8.464	-7.813	-4.577	-3.792	-4.475	-5.226	-5.678	-5.637	-5.753	-7.267
C_5^0	-4.200	-5.206	-3.027	-.370	.423	2.394	3.798	6.361	6.855	3.059	-.658	-2.626
C_6^0	2.719	2.933	4.697	5.245	6.942	7.414	7.550	7.841	5.643	3.167	1.321	4.151
C_7^0	7.528	9.353	6.928	5.132	.506	-3.346	-4.715	-4.899	-1.912	.003	5.156	6.946
C_8^0	-5.707	-4.183	-3.671	-1.914	-4.612	-4.349	-3.440	-3.244	-7.136	-7.810	-6.087	-5.554
C_9^0	-2.440	-2.964	-3.988	-4.177	.228	3.424	3.600	3.751	1.645	.339	-1.468	-3.243
C_{10}^0	.101	-1.419	1.218	.908	.464	.055	-1.504	1.926	4.108	3.969	1.781	1.566
C_{11}^0	1.448	.442	.618	1.283	1.975	1.039	.398	1.338	-.930	.857	2.639	1.254
C_{12}^0	.825	-.000	1.436	1.171	-.085	1.223	.314	-1.545	-.462	-.466	-2.022	.489

^aFor limb-darkening model.

TABLE III.- SPHERICAL HARMONIC (NONAXISYMMETRIC) COEFFICIENTS OF LONGWAVE RADIANT EXITANCE ($W\text{-m}^{-2}$)

[Cosine terms are below staircase and sine terms are above; coefficients are for 12th degree expansion at top of atmosphere; results are for limb-darkening model]

(a) July 1975

	12	11	10	9	8	7	6	5	4	3	2	1	$\frac{m}{n}$
	.561	.013	.112	-.842	-.305	-.130	.329	-.697	-1.243	-.205	.166	-.660	12
1	2.996	-.078	-1.129	.776	-1.047	-.630	.021	.263	1.149	-.103	.568	.356	11
2	4.639	4.104	-1.109	.923	-.045	-.951	.518	-.006	1.620	1.066	1.576	1.215	10
3	1.706	2.954	-.971	-.031	-.222	.651	1.267	-.398	-.146	1.114	.342	-.538	9
4	-.554	-1.382	-2.284	-2.923	-1.386	1.498	1.105	.012	-1.769	-.931	-1.436	.224	8
5	-5.142	-3.437	.325	-2.242	-1.140	-.210	-.420	-.215	-1.372	-1.946	-1.981	.101	7
6	-2.326	-1.809	2.236	-.193	-.284	1.871	-.817	.121	-1.136	.756	.745	.895	6
7	1.706	.367	.403	.530	.590	2.045	.746	-1.062	1.058	2.731	.546	-3.562	5
8	1.199	1.988	-1.799	1.527	.527	.727	1.018	2.431	.472	-.588	.598	3.352	4
9	.451	2.770	.034	.212	-.359	.250	-.061	-.045	-.422	-1.552	3.266	3.469	3
10	.318	1.067	1.373	-.335	-.309	-.263	.905	-1.499	.411	-.923	5.222	-.636	2
11	-.277	-2.851	.091	-.126	-.362	.274	.508	-1.480	-.268	-.472	.409	-2.953	1
12	.194	-1.889	-1.180	.849	.177	.262	.298	-.324	.204	-.525	.299	.596	
$\frac{n}{m}$	1	2	3	4	5	6	7	8	9	10	11	12	

TABLE III.- Continued

(b) August 1975

														$\frac{m}{n}$
		12	11	10	9	8	7	6	5	4	3	2	1	
C_n^m		-.103	-.158	-.202	.327	-.233	.375	.044	.150	-.596	-.154	.493	.003	12
	1	3.173	.837	-.351	.329	-.072	-.527	.349	.762	1.166	.085	-.466	.227	11
	2	3.586	4.425	.043	-.062	.673	-.187	.493	-.434	.965	.463	.893	2.476	10
	3	1.080	2.713	1.124	-.524	.835	.487	.906	-.859	-.042	.421	.222	-.352	9
	4	-1.134	-2.459	-1.078	-2.795	.156	.151	-.204	-.804	-1.090	-.186	-.115	.319	8
	5	-3.404	-2.701	.230	-1.218	-1.664	.292	-1.090	.023	-.181	-1.678	-.067	-.664	7
	6	-.144	-.075	2.057	.529	.960	1.050	-1.414	.513	.510	.585	-.576	-1.014	6
	7	1.982	.590	.853	.884	.749	.321	1.503	-1.217	-.204	2.848	-.848	-3.639	5
	8	-.345	1.713	-1.306	.618	-.847	.787	1.701	.689	-.133	-.303	.550	3.993	4
	9	-.855	1.099	-1.443	-.245	-.030	.100	.194	-.835	1.051	-1.437	2.803	4.431	3
	10	.116	.637	.841	-.255	.655	-.337	-.357	-1.099	1.179	.095	3.077	-1.380	2
	11	.494	-1.913	1.054	.323	-.289	-.013	-.036	-.987	-.260	-.369	.112	-3.134	1
12	1.564	-1.891	-.328	.519	-.091	.433	-.136	.162	.401	.879	.539	.729		
$\frac{n}{m}$	1	2	3	4	5	6	7	8	9	10	11	12		

S_n^m

TABLE III.- Continued

(c) September 1975

	12	11	10	9	8	7	6	5	4	3	2	1	$\frac{m}{n}$
	-.021	-.323	.126	-.181	-.260	.012	.682	-.876	-.718	.739	-.104	.104	12
1	1.414	-.010	-.277	.009	-.556	.183	-.401	-.096	.221	.155	-.586	.246	11
2	2.903	4.495	.672	-.054	-.593	-.084	-.628	.635	.681	-.076	.029	1.696	10
3	.744	2.165	.783	.300	.043	.783	.900	.152	.214	.781	.041	-1.894	9
4	-.439	-2.707	-.475	-4.352	-.357	-.134	.795	-.315	-.784	.114	.278	.430	8
5	-2.953	-1.898	.496	-1.527	-2.711	.121	.322	.798	-.507	-1.372	-.144	1.631	7
6	.044	.882	1.931	.493	.179	1.648	-.352	.601	.380	.775	-.042	1.229	6
7	1.571	-.440	-.283	-.360	1.091	1.629	1.680	-1.394	-.905	2.233	-.159	-3.473	5
8	-.654	-.369	-1.030	-.435	-.858	.598	.511	1.301	-1.312	-.236	-.109	2.545	4
9	-.521	1.373	.342	.072	-.898	-.307	-1.212	-.041	.300	-.369	3.223	2.695	3
10	.402	.821	.682	-.298	-.017	-.338	-.550	-1.693	-.648	-.905	4.746	-.526	2
11	-.243	-1.335	-.613	.302	.382	.241	.013	-.176	-.922	-.703	.062	-2.551	1
12	.528	-.559	-.482	.902	-.003	.169	.101	.013	-.293	-.554	.219	.525	
$\frac{n}{m}$	1	2	3	4	5	6	7	8	9	10	11	12	

TABLE III.- Continued

(d) October 1975

														$\frac{m}{n}$
		12	11	10	9	8	7	6	5	4	3	2	1	
C_n^m		.087	-.151	.553	.317	-.233	.152	-.300	.049	.059	.403	-.734	-.190	12
	1	3.357	.453	.693	-.766	-.713	.414	-1.005	.363	-.533	-.419	-.407	.476	11
	2	2.737	3.019	.858	-.289	-.401	-.000	-.547	1.141	.438	-.237	.948	1.402	10
	3	-.026	2.617	-.214	-.487	-.468	-.583	.381	-1.540	.588	1.385	1.209	-1.922	9
	4	-1.145	-2.922	-.307	-1.557	.107	.019	.599	-1.062	-.774	1.238	.515	-.528	8
	5	-2.286	-1.679	-.352	.312	-.830	1.229	.129	1.382	.113	-2.218	-.911	.922	7
	6	.832	2.848	1.135	1.217	.286	1.499	-1.080	-.593	2.246	.101	-.587	1.801	6
	7	1.905	.525	.202	1.017	1.339	.601	1.636	-1.924	-1.229	1.394	-.582	-2.329	5
	8	-.632	.194	-.290	.034	-.310	-.149	-.437	.319	-3.324	-.115	-2.134	1.229	4
	9	-.925	.819	.513	-.755	-.943	-.444	.058	.507	.329	.874	2.509	.543	3
	10	.652	-.762	.093	-.441	.196	-.683	.066	-1.998	-.867	-.215	6.525	.150	2
	11	-.364	-1.739	-.648	.213	.729	-.101	.981	-.040	.456	-.136	-.087	-1.091	1
12	.831	.391	.191	.959	-.682	.002	.556	.395	.426	1.509	.299	.776		
$\frac{n}{m}$	1	2	3	4	5	6	7	8	9	10	11	12		

S_n^m

TABLE III.- Continued

(e) November 1975

		12	11	10	9	8	7	6	5	4	3	2	1	$\frac{m}{n}$
C_{mn}^m		.975	-.104	.134	.739	-.194	.424	.311	-.895	.019	1.052	-1.096	.075	12
	1	1.504	.826	-.241	-.030	.014	.151	-.117	-.269	-.840	-.622	-.768	1.657	11
	2	1.887	.772	.508	.154	-.518	-.089	.222	.435	-.259	-1.325	1.635	2.276	10
	3	-.035	2.466	.223	-.237	-.879	-.531	-.389	-.544	1.363	1.021	1.649	-2.389	9
	4	.295	-.030	-1.254	-1.339	-.354	-.172	.365	-1.482	-.333	2.226	-.355	-1.413	8
	5	-.711	-.209	-.192	-.668	-.188	.340	.885	.827	-1.018	-.675	-.009	1.704	7
	6	.486	2.837	1.298	.816	-.320	1.469	.111	.337	1.706	-.754	2.076	1.908	6
	7	1.427	1.085	-.572	.283	1.623	.878	.297	-3.141	.039	.454	-.743	-1.649	5
	8	-.657	-.645	-1.337	-1.146	.150	.067	-.480	.651	-2.510	.917	-3.722	.723	4
	9	-.837	-.399	.677	.185	-1.096	-.459	-.324	-.178	-.494	.772	.923	.083	3
	10	1.082	.230	.284	.786	-.003	-.126	-.397	-1.020	-1.179	.265	4.527	-.768	2
	11	.106	-.806	-1.664	.179	.504	.167	.735	1.403	-.555	.013	.649	-.463	1
12	-.800	.346	.107	.976	.223	.156	-.003	.536	.800	.743	-.041	-.266		
$\frac{n}{m}$		1	2	3	4	5	6	7	8	9	10	11	12	

TABLE III.- Continued

(f) December 1975

	12	11	10	9	8	7	6	5	4	3	2	1	$\frac{m}{n}$
	1.034	-.526	.686	-.670	.264	.355	.207	-.398	.196	1.088	.243	-.021	12
1	1.814	.239	-.601	-.262	.579	.284	-.019	-.204	-.646	.435	-.511	2.086	11
2	.495	1.016	1.493	-.416	.249	-.056	-.110	.544	.036	-1.310	.522	2.055	10
3	-.111	3.146	.077	-.533	.119	-.357	-.641	-1.084	1.936	-.308	.844	-2.688	9
4	1.394	.022	-2.405	2.759	.562	-.696	.038	-.719	-1.076	2.366	-.784	-.560	8
5	-.826	.298	-.230	-1.460	-.329	.581	.256	1.878	-2.098	-.904	-.418	2.587	7
6	.376	3.381	2.797	-.969	.463	.245	.193	.691	2.058	-3.296	3.124	2.391	6
7	.480	.933	-.064	.428	.579	-.677	.249	-2.359	-.012	.755	.102	-2.055	5
8	-1.398	-1.854	-1.940	-1.209	-.434	.109	-.056	1.703	-3.979	2.227	-3.666	-.321	4
9	-.457	-1.022	.187	.341	-.934	-.376	-.670	.469	.390	-.312	.306	1.042	3
10	1.214	.668	-.333	1.535	.177	.099	.073	-1.145	-.546	-.840	4.051	.826	2
11	.294	.070	-.695	.579	.668	.422	1.215	.334	-.207	.520	-.760	-2.102	1
12	-.619	-.210	1.127	-.160	.002	-.060	-.191	.604	.410	-.930	.163	.906	
$\frac{n}{m}$	1	2	3	4	5	6	7	8	9	10	11	12	

C_n^m

S_n^m

TABLE III.- Continued

(g) January 1976

		12	11	10	9	8	7	6	5	4	3	2	1	$\frac{m}{n}$
		.410	-1.128	-.315	.841	.162	-.201	1.251	-.470	.247	1.151	.222	.330	12
C_n^m	1	1.154	.503	-.669	.971	.236	.010	-.473	.872	-.431	.908	.103	1.231	11
	2	.341	.653	-.036	-.408	-.413	.530	-1.014	1.003	.098	-1.087	.327	2.179	10
	3	.161	2.558	.310	-.492	-.659	.341	-.066	-1.183	2.501	-.630	.514	-1.653	9
	4	1.045	.837	-3.478	2.506	-.005	-.161	.593	-1.500	.167	1.914	-.932	-1.911	8
	5	-1.991	.417	.742	-.854	.503	-.060	-.199	.924	-3.438	-.827	-.248	1.336	7
	6	-.397	2.080	3.359	.152	-.457	-.298	-1.600	1.975	.786	-3.111	3.057	2.763	6
	7	1.865	.077	.077	.370	.861	.930	1.982	-2.145	1.703	.649	.826	-1.831	5
	8	-.423	-1.358	-2.256	-1.263	.043	.343	.630	.751	-3.664	1.580	-2.037	-.409	4
	9	-.995	-.218	-1.785	.431	-1.275	-1.023	-1.614	.439	-.771	-.574	.053	.751	3
	10	1.064	1.121	.012	1.433	.094	.609	-1.183	-.050	-.819	.075	2.319	.723	2
	11	.611	-.376	1.203	-.279	.560	1.012	.221	.104	.120	-.218	.745	-1.027	1
	12	-.319	-.034	.614	-.286	-.130	-.407	.562	-1.108	1.159	.032	-.484	-1.299	
$\frac{n}{m}$		1	2	3	4	5	6	7	8	9	10	11	12	

 S_n^m

TABLE III.- Continued

(h) February 1976

		12	11	10	9	8	7	6	5	4	3	2	1	$\frac{m}{n}$
		.210	-1.183	.197	-.160	.068	.402	.417	-.828	.728	1.245	-1.060	-.518	12
$C_{m,n}^m$	1	1.869	.840	-.576	-.090	.145	1.030	-.797	.317	-.522	1.082	-.538	.489	11
	2	.690	-2.107	.692	-.084	-.906	.357	.389	.988	-.448	-1.368	1.811	2.314	10
	3	.319	2.229	1.780	.277	-.982	-.169	-.628	-.498	1.846	-.471	.575	-1.376	9
	4	.479	2.923	-2.418	2.732	-.512	.435	-.165	-1.200	.761	2.458	-1.759	-1.082	8
	5	-.978	.533	.440	-1.105	-1.238	-.782	.963	1.431	-1.062	-.939	-.417	.296	7
	6	.582	1.512	4.196	-.944	-.334	-.718	-1.555	1.243	1.201	-2.612	4.009	2.647	6
	7	1.748	.094	-.395	1.284	1.363	-.148	.390	-3.316	.152	1.137	1.892	-.130	5
	8	.359	-1.253	-2.143	-.524	-.210	-.228	-.074	.010	-2.217	1.543	-3.014	.198	4
	9	-1.619	.409	-.021	-.139	-1.510	-.298	-.416	.166	.756	-1.195	-.374	-.754	3
	10	1.116	1.237	-.552	1.399	.042	.102	-.648	.205	-.442	.919	2.976	-.470	2
	11	.094	-1.104	-.168	.373	.761	-.034	.034	.438	-.062	-1.382	1.287	-.969	1
	12	-.792	-.552	.270	-.997	-.032	-.626	.249	.725	.340	-.378	-.212	-1.808	
$\frac{n}{m}$		1	2	3	4	5	6	7	8	9	10	11	12	

$S_{m,n}^m$

TABLE III.- Continued

(i) March 1976

		12	11	10	9	8	7	6	5	4	3	2	1	$\frac{m}{n}$
			1.258	-.231	-.189	.621	.326	.768	.761	-.276	-.243	.174	-1.539	.263
C_n^m	1	2.067	.859	.857	.264	-.627	.565	-.511	.354	-.496	.492	.872	-1.153	11
	2	1.122	-1.791	.421	.760	-.292	-.162	.036	.337	.383	-1.160	2.918	2.213	10
	3	-.146	.951	.760	.977	.595	-1.027	-.051	-1.013	.825	.078	.170	-1.136	9
	4	.549	2.554	-1.444	1.783	.157	-.763	.385	-1.638	-1.652	1.851	-2.549	-1.148	8
	5	-.388	1.298	1.018	-.654	-.172	2.418	.547	2.115	-.934	-1.295	.077	-1.241	7
	6	.109	-.438	2.355	-.336	-.522	1.078	-1.089	1.513	2.201	-2.184	4.603	3.380	6
	7	.214	-1.462	-1.094	.275	2.061	-.011	-.804	-3.280	.041	1.466	1.071	.932	5
	8	-.398	.204	-.369	-.200	-.498	-.197	-.131	.717	-3.223	.223	-3.054	1.096	4
	9	.071	1.879	1.192	.221	-.347	-.273	.560	.199	1.122	-1.324	.025	-1.318	3
	10	1.474	.630	-.430	1.007	.493	.364	-.074	-.779	.633	.411	2.261	-.481	2
	11	-.327	-.846	-.391	.690	-.051	.188	-.055	.700	.579	-.757	.029	.332	1
	12	-.092	-.357	.894	-.114	.316	-.194	-.169	-.506	1.066	.170	-.384	.753	
$\frac{n}{m}$	1	2	3	4	5	6	7	8	9	10	11	12		

 S_n^m

TABLE III.- Continued

(j) April 1976

	12	11	10	9	8	7	6	5	4	3	2	1	$\frac{m}{n}$
	.026	-1.477	-.357	-.451	.154	-.461	-.445	-.186	.027	.416	-1.300	1.216	12
1	2.628	-.349	-.406	-.506	-.213	.719	.703	.351	-.354	.383	-.682	.176	11
2	1.542	-1.455	.307	.437	.217	-.340	.342	.491	-.363	-1.162	2.096	1.348	10
3	.094	-.815	1.133	.148	-.387	-1.027	-.542	-.876	.244	.172	1.111	-1.763	9
4	.227	1.432	-1.713	.273	-.492	-.283	.151	-.933	-.451	1.673	-2.063	-.653	8
5	-.684	.057	-.549	.269	-1.244	1.656	.257	1.071	-.367	-1.225	-.549	-.577	7
6	.220	-.799	3.118	-.158	.149	.861	-.544	.053	1.118	-1.541	3.175	2.997	6
7	.501	-.775	.070	.051	2.185	-.702	-.723	-3.366	.290	2.037	.731	.179	5
8	-1.087	.456	-.837	.031	.459	-.156	-.019	1.285	-2.357	.757	-1.029	1.301	4
9	.005	.960	.642	-.335	-.894	.474	.012	-.020	.058	-.934	1.630	-1.502	3
10	1.389	.659	-.107	.118	-.208	-.510	-.293	-.941	-.774	-1.913	.950	.077	2
11	-.244	-1.211	-.223	.241	.250	-.279	.361	.579	-.047	-.059	-1.371	.200	1
12	-.154	-.939	.536	.476	-.016	.179	.207	-.197	.347	1.582	-.722	-.341	
$\frac{n}{m}$	1	2	3	4	5	6	7	8	9	10	11	12	

C_{n}^m

S_{n}^m

TABLE III.- Continued

(k) May 1976

	12	11	10	9	8	7	6	5	4	3	2	1	$\frac{m}{n}$
	.397	.073	.958	-.230	-.386	-.089	.442	.008	-.798	.174	.016	.718	12
1	3.111	.616	.030	.652	.486	.311	.047	-.660	-.381	-.582	.006	-.128	11
2	2.977	.420	.078	-.700	.490	.021	-.208	.346	.013	-.361	.214	1.824	10
3	-.199	-.266	.462	.385	-.591	-.216	-.061	-.308	.681	1.162	.721	-.567	9
4	.045	-.420	-2.444	-.304	-.838	-.165	.220	-.367	-.538	1.061	-.373	-.202	8
5	-1.187	-1.494	.482	.104	.827	-.074	.989	.987	-.404	-1.196	-.830	-.705	7
6	.062	.185	3.010	.636	.391	.415	.796	-.355	1.153	-.250	1.277	1.689	6
7	.417	1.132	-.319	.316	.342	.019	-.742	-1.304	-1.389	.931	.702	-1.943	5
8	-.415	1.578	-1.827	-.172	-.360	1.154	.151	-.255	-2.768	-.097	-.890	1.729	4
9	-.927	.506	.240	.045	-1.162	.371	-.310	-1.534	-.344	-.278	1.254	-.572	3
10	.368	.631	.414	.352	-.136	-.967	-.758	-.882	-.579	.166	3.455	.285	2
11	.846	-1.434	-.360	.317	.329	.293	.615	.592	.817	-.433	.166	.981	1
12	.432	-.931	.553	.089	.527	.579	-.417	1.351	.277	.279	-.217	.249	
$\frac{n}{m}$	1	2	3	4	5	6	7	8	9	10	11	12	

TABLE III.- Concluded

(1) June 1976

														$\frac{m}{n}$
		12	11	10	9	8	7	6	5	4	3	2	1	
C_n^m		-.481	-.585	-1.568	-.618	-.508	-.507	-.240	.393	-1.388	.439	-.442	.400	12
	1	4.919	.332	-.117	-.039	-.957	-.413	-.425	-.018	.014	-.323	.213	-.314	11
	2	4.066	2.849	1.567	-1.614	.063	.762	-.267	-.183	1.253	.268	1.568	1.732	10
	3	-1.161	2.011	.364	-.408	.485	.158	.149	-.333	1.396	.698	1.084	-.950	9
	4	-.987	-1.707	-1.025	-3.683	-.505	.367	.460	-1.053	.196	-.589	.091	-1.388	8
	5	-2.019	-3.384	-.934	-1.472	-.687	-.087	.328	-.100	-.228	-1.754	-.189	-.255	7
	6	-1.348	-.525	1.751	.984	-.165	.885	.283	.812	-1.249	-.104	-.958	2.084	6
	7	.745	.948	1.301	1.403	.657	.412	-.196	-.423	-2.077	2.313	-2.675	-2.773	5
	8	.468	2.182	-1.241	.968	.061	1.466	.292	-.520	-1.192	.251	.200	1.495	4
	9	.744	1.125	-.586	.041	-.005	.274	.530	-.432	1.199	-.389	5.304	1.741	3
	10	.840	-.586	.941	-.442	.557	-.070	1.051	-.954	-.360	-.424	5.778	1.262	2
	11	-.511	-1.621	-.159	.004	.413	.099	.364	-1.250	-.974	.176	-.765	-.512	1
12	.196	.486	.313	.979	-.029	.466	-.652	-.483	.374	1.011	-1.429	-.322		
$\frac{n}{m}$	1	2	3	4	5	6	7	8	9	10	11	12		

S_n^m

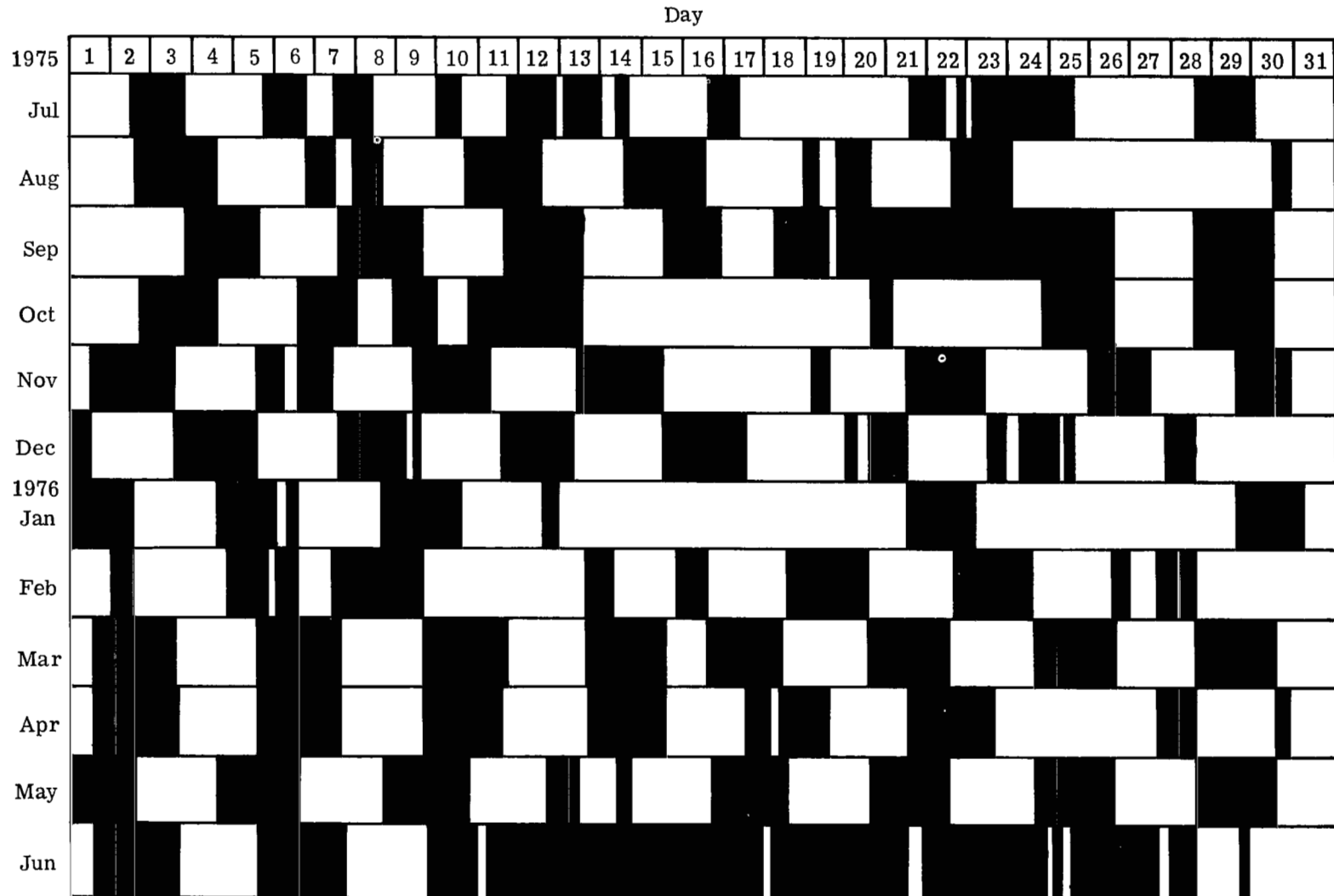


Figure 1.- Time periods for longwave radiation measurements from Nimbus 6 (dark bands) for 12-month period from July 1975 through June 1976.

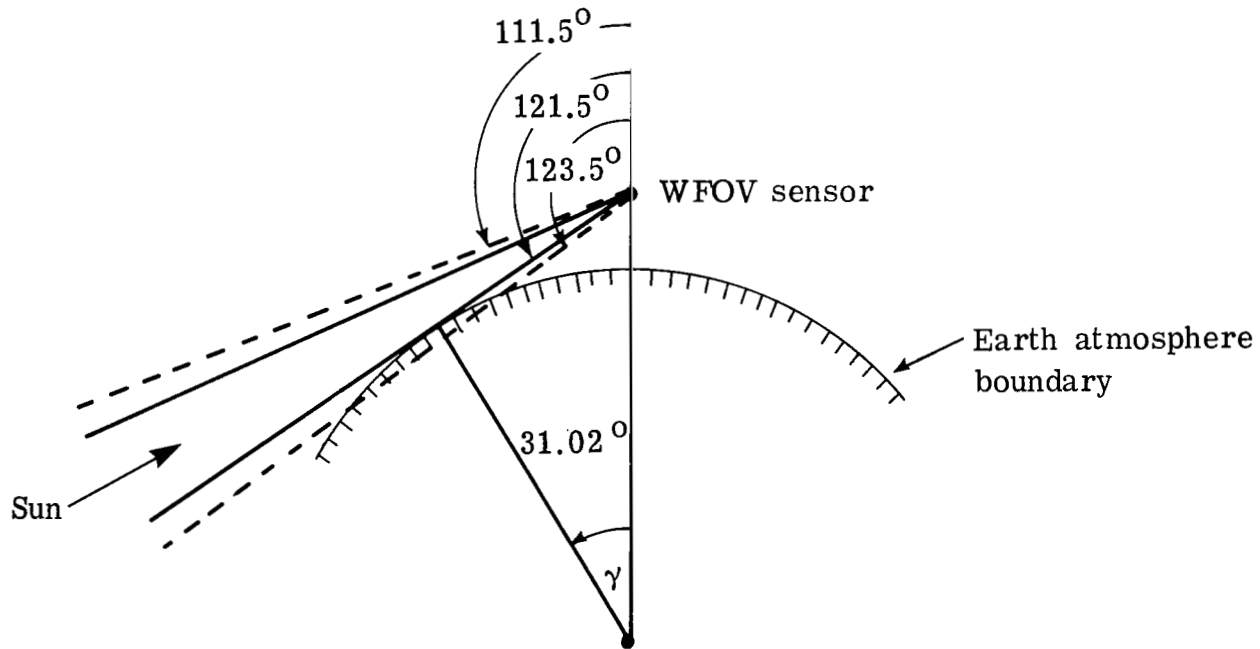


Figure 2.- Range of Sun zenith angle for which wide-field-of-view (WFOV) sensor measurements were deleted (111.5° to 123.5°).

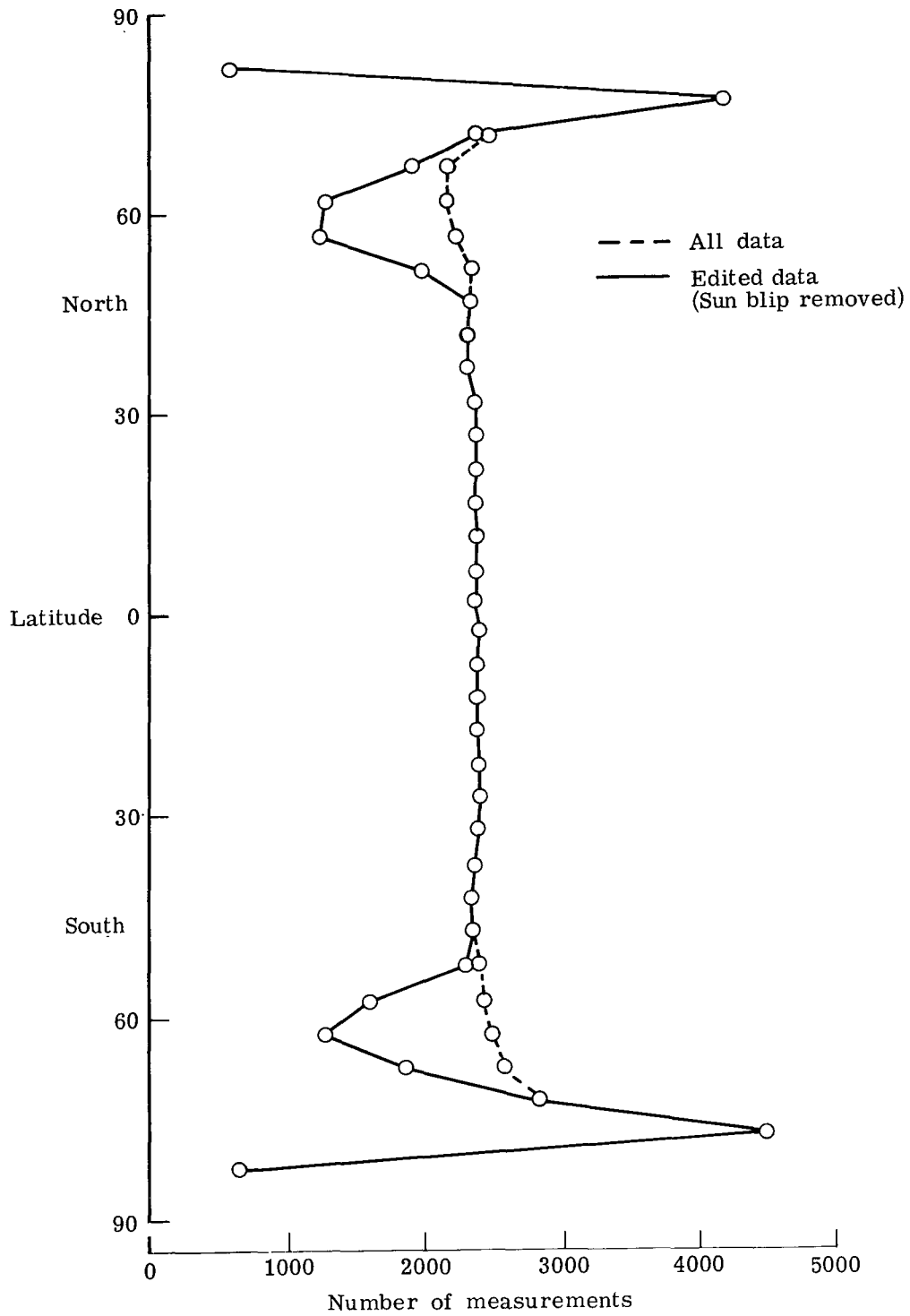


Figure 3.- Zonal sampling plot for September, showing zonal deficiency in number of measurements due to removal of Sun contaminated measurements.

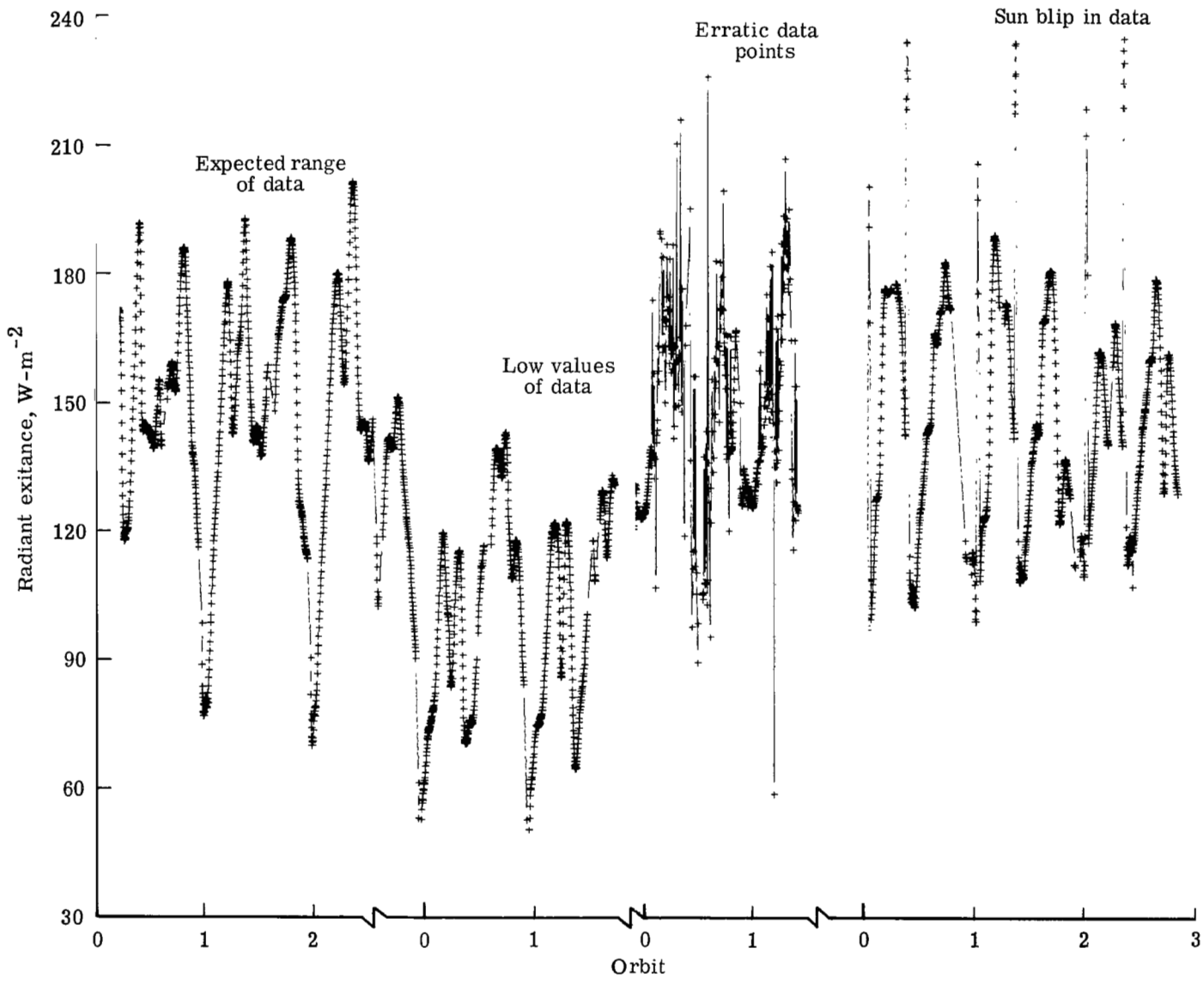


Figure 4.- Composite plot of raw longwave radiant exitance showing some anomalies in data.

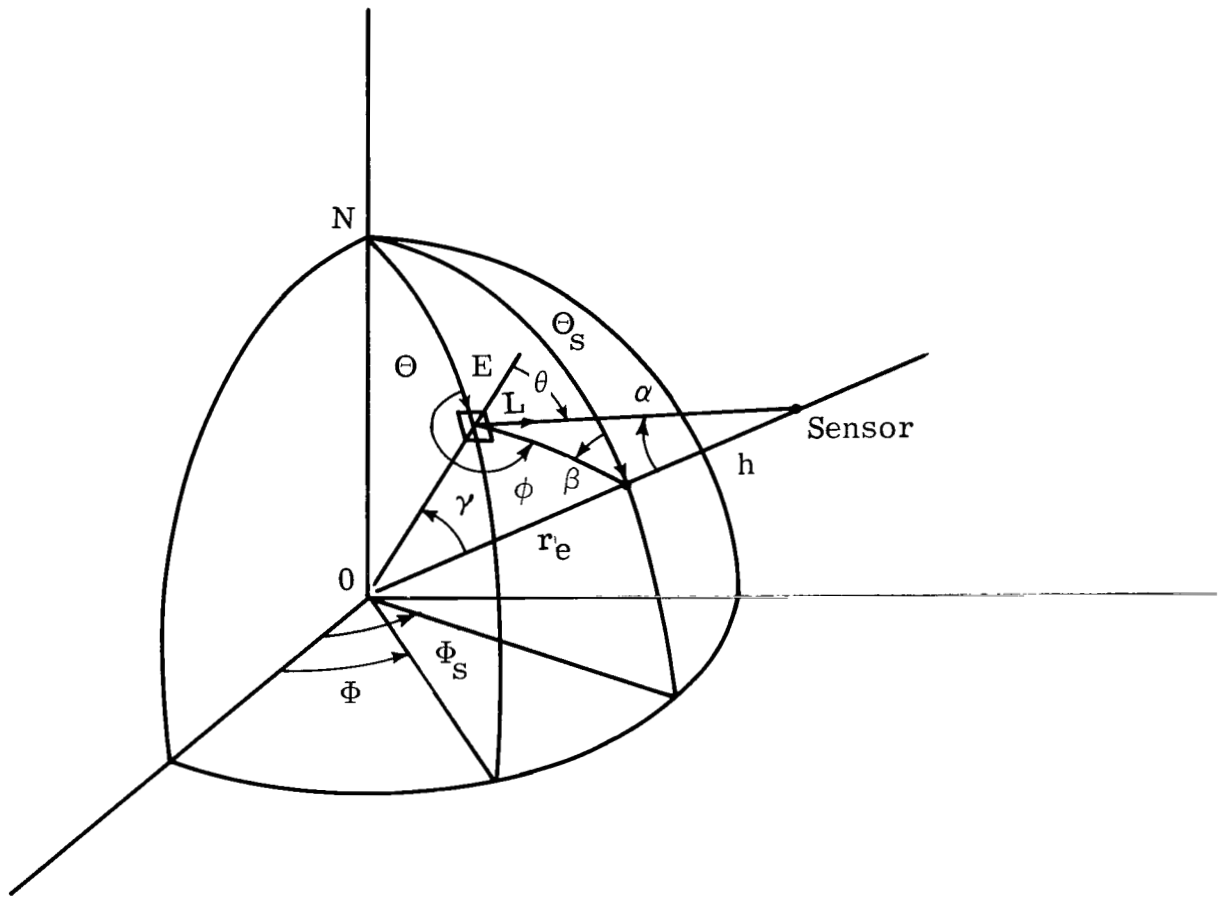


Figure 5.- Earth satellite geometry.

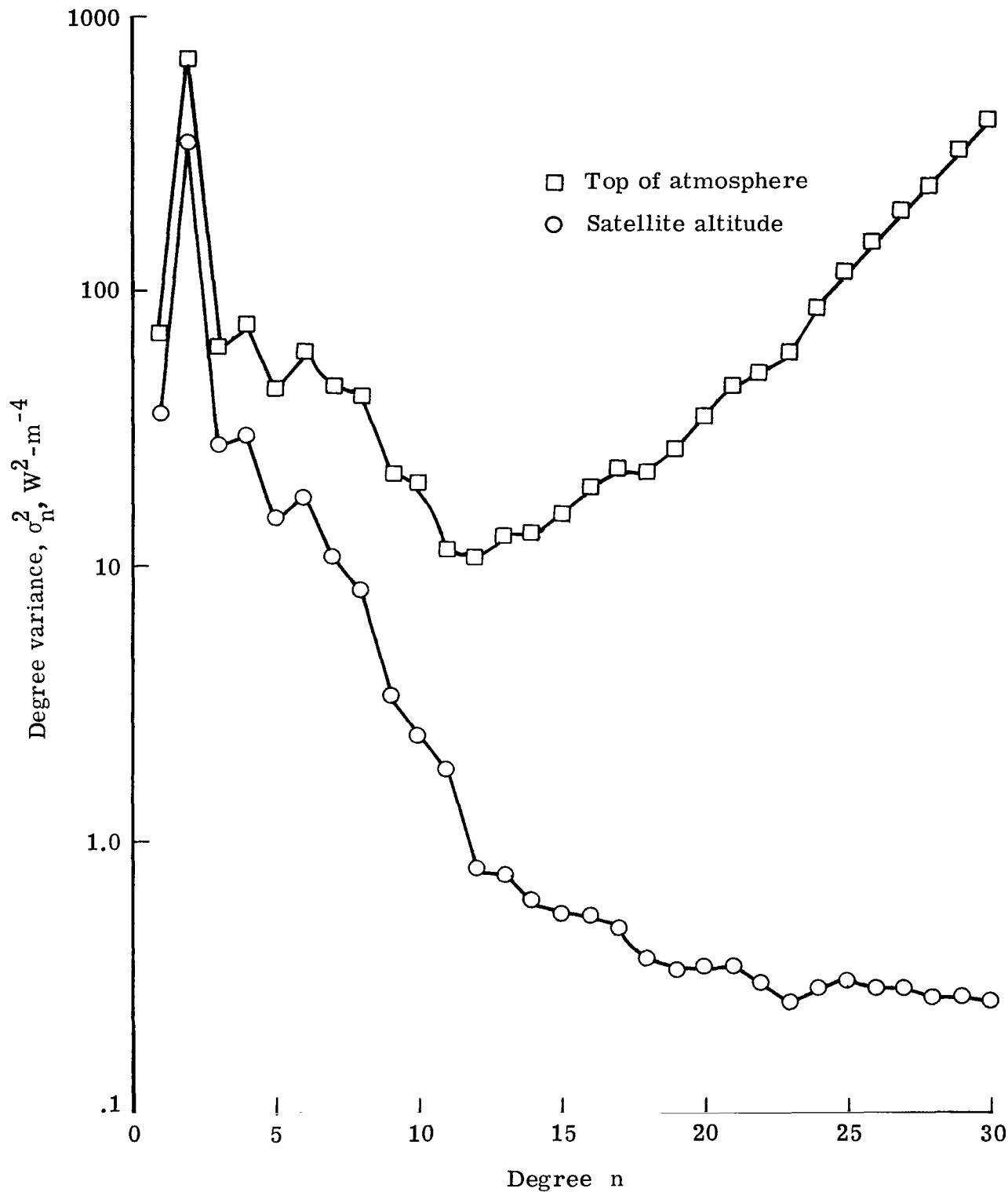


Figure 6.- Degree variance plot for average of 12-month data set.

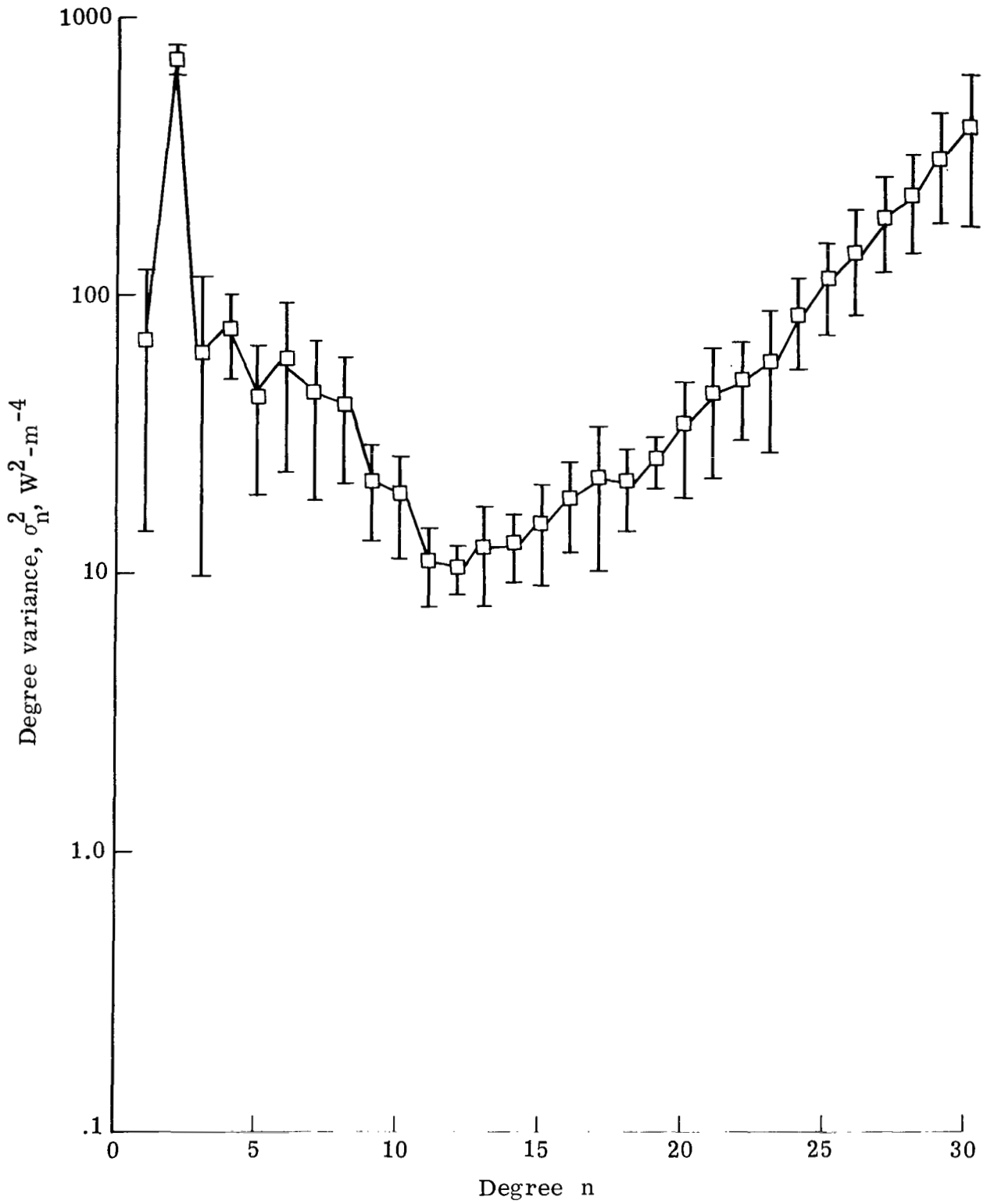
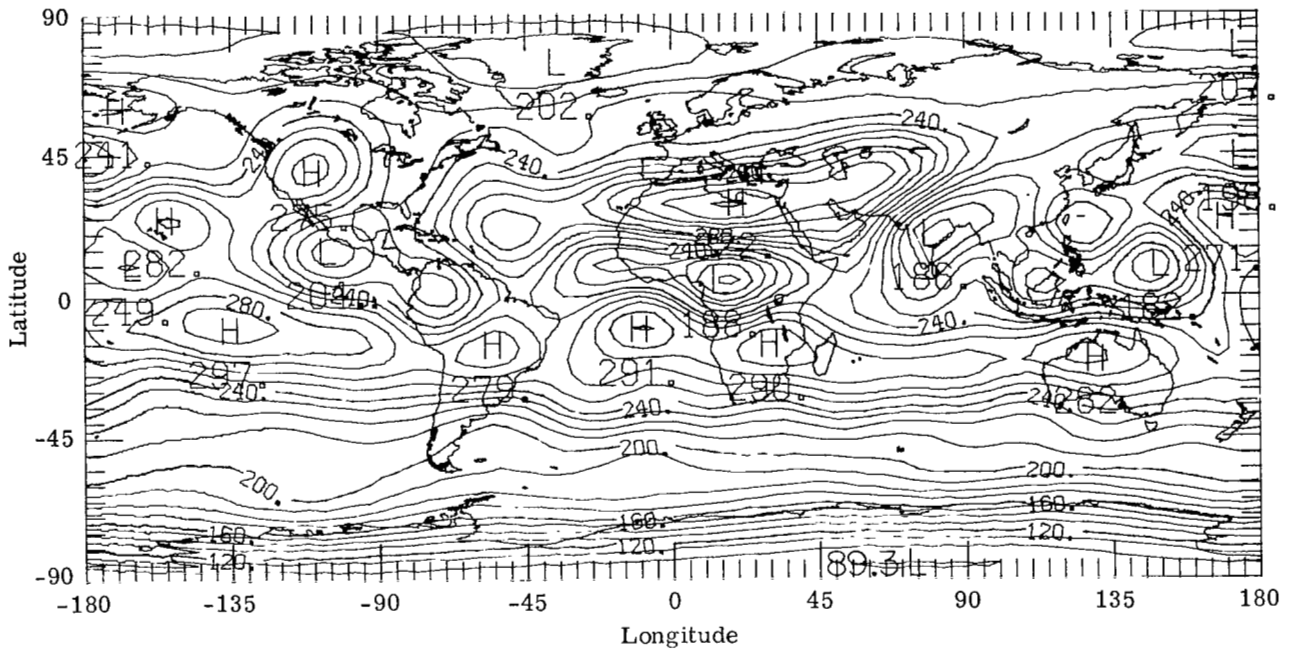
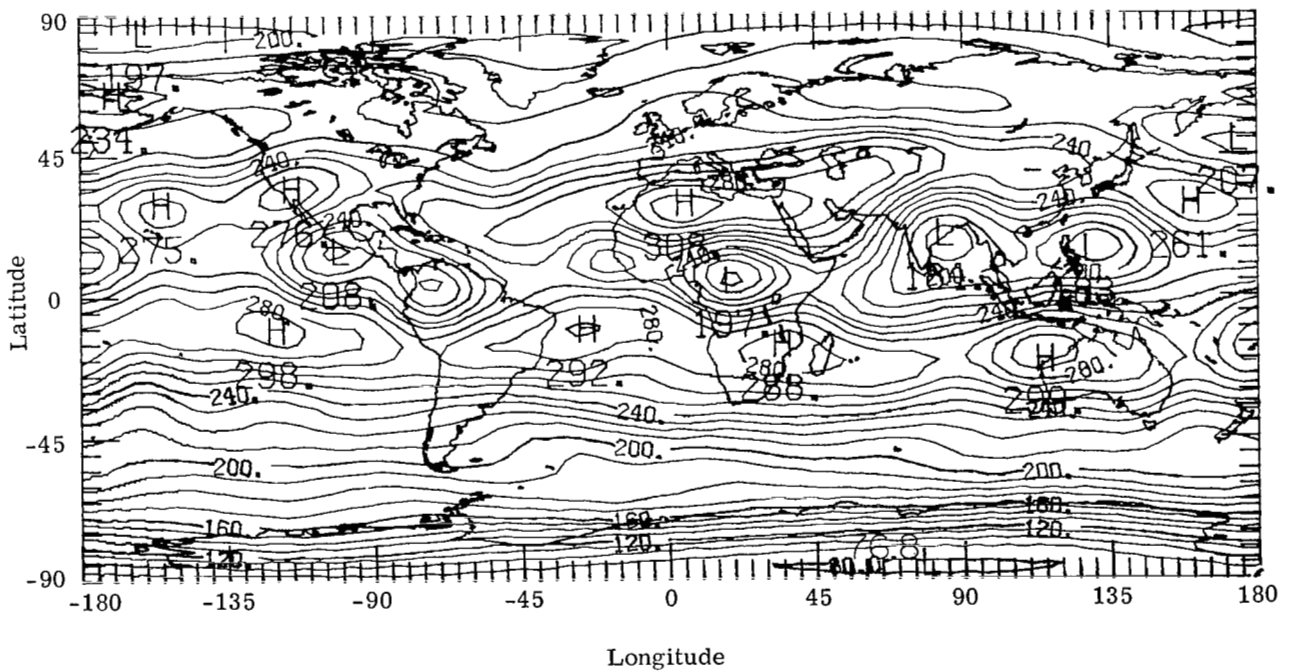


Figure 7.- Standard deviation of average degree variance over 12 months at top of atmosphere for degree 1 to 30.

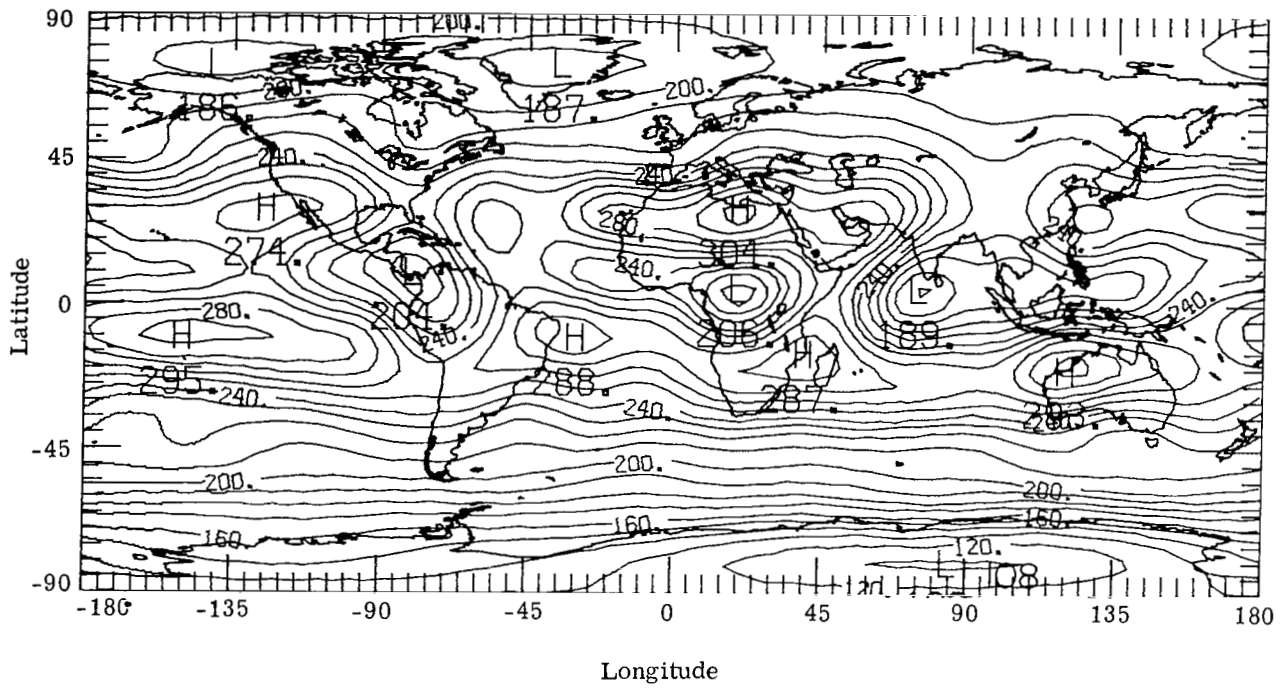


(a) July 1975.

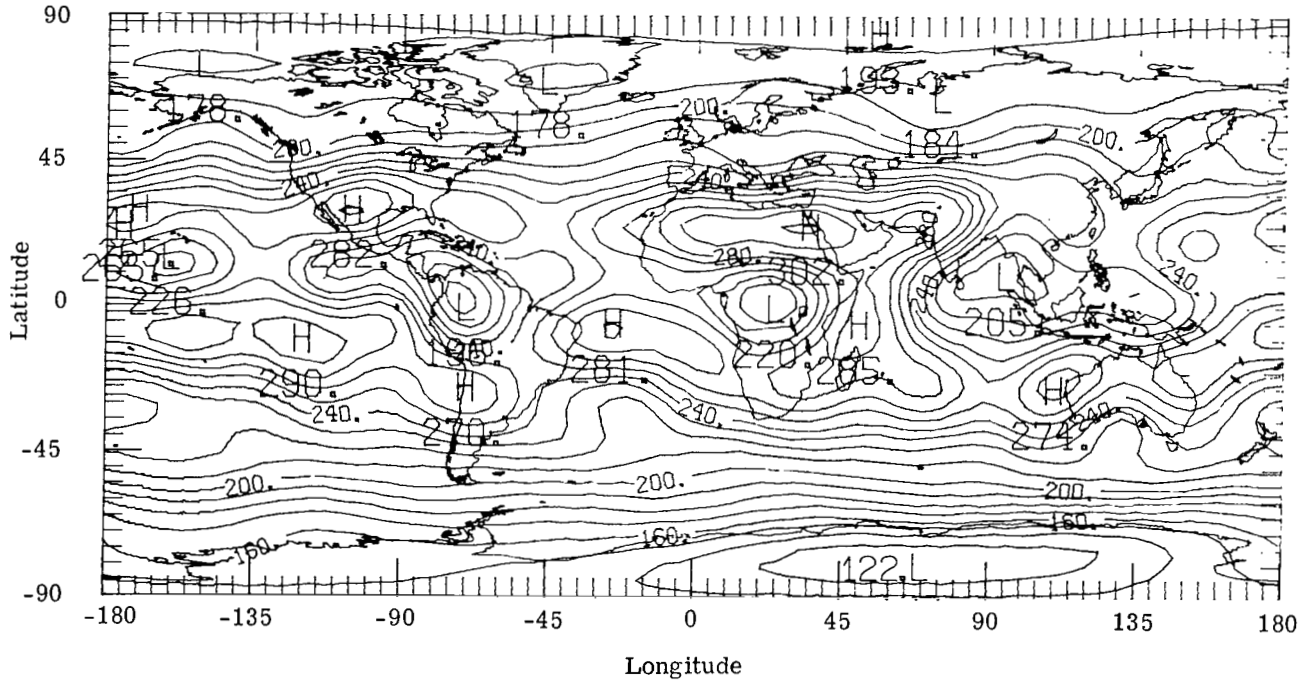


(b) August 1975.

Figure 8.- Geographical distribution of Earth emitted radiant exitance at top of atmosphere ($W\cdot m^{-2}$) for 12-month period.

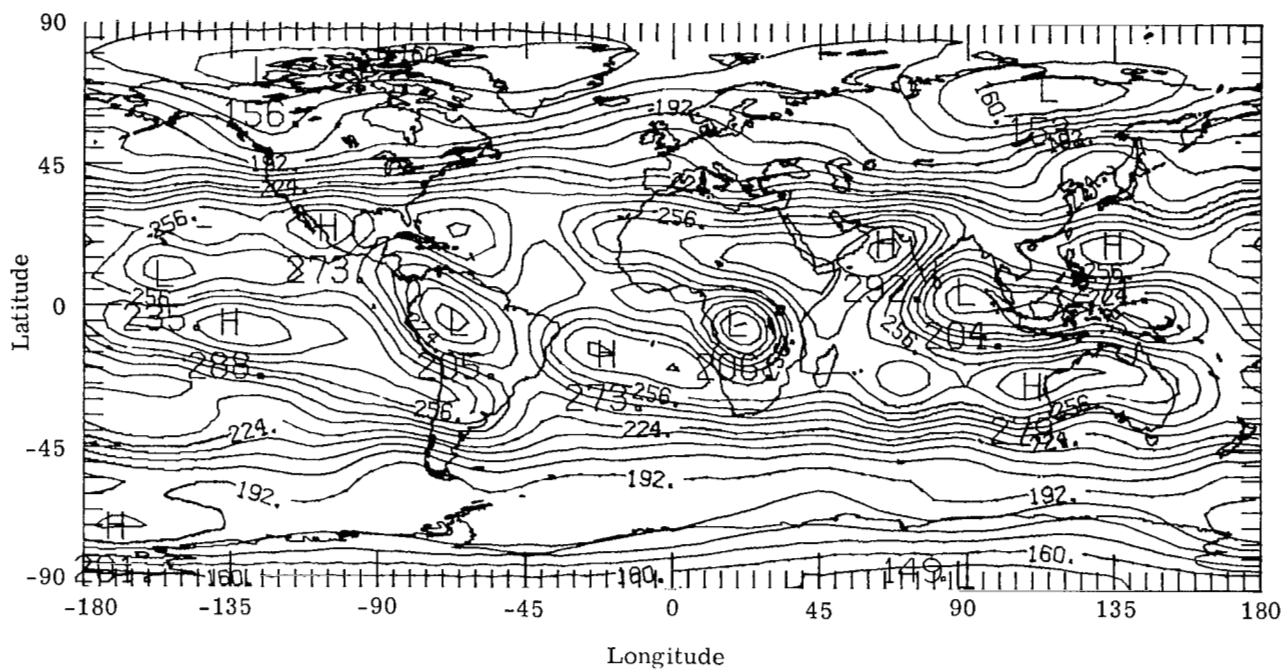


(c) September 1975.

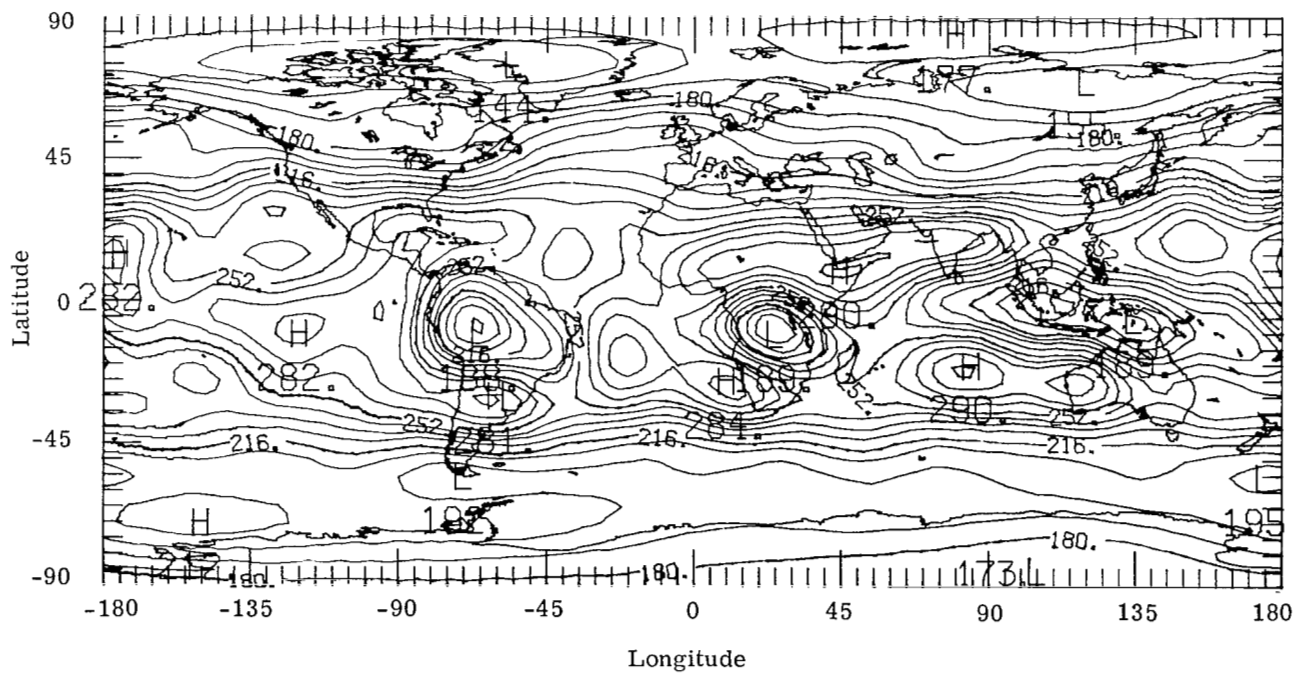


(d) October 1975.

Figure 8.- Continued.

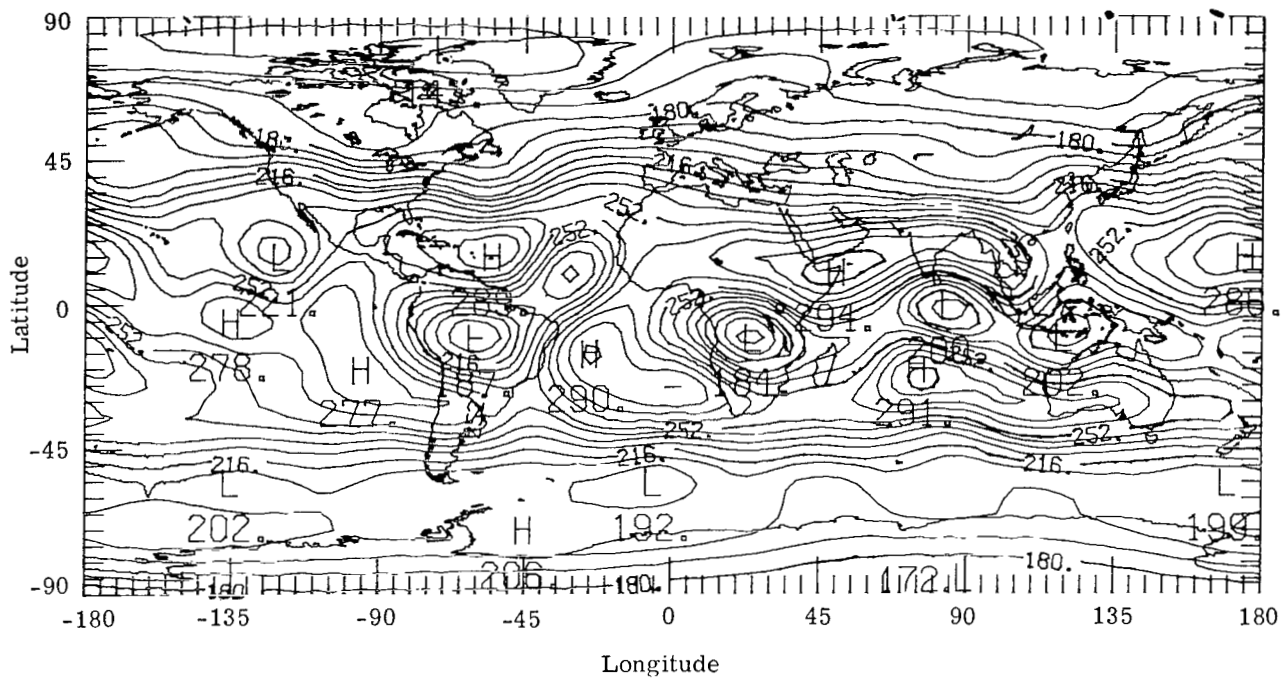


(e) November 1975.

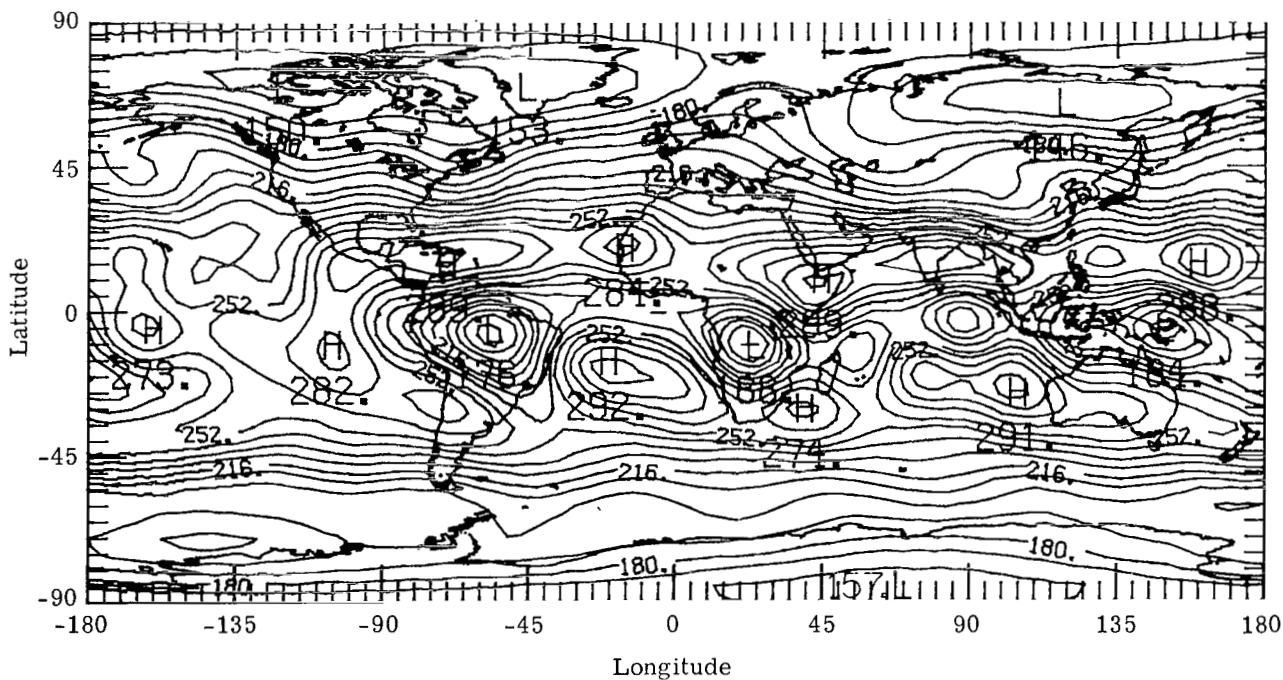


(f) December 1975.

Figure 8.- Continued.

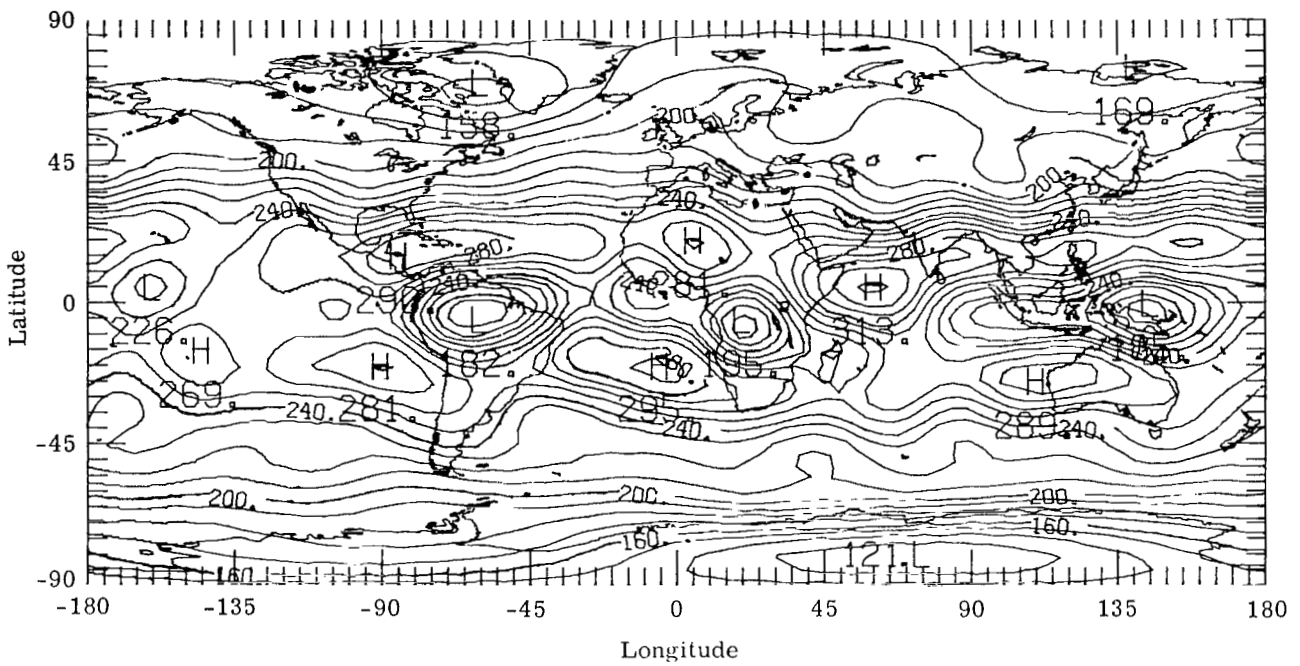


(g) January 1976.

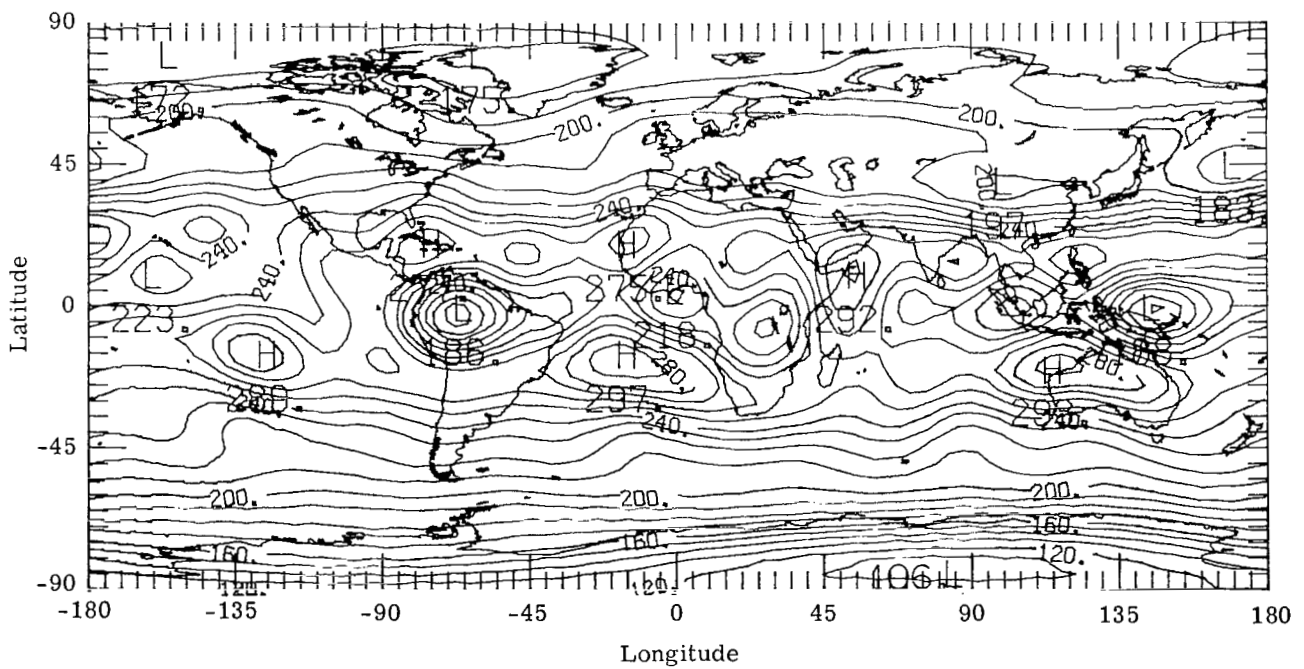


(h) February 1976.

Figure 8.- Continued.

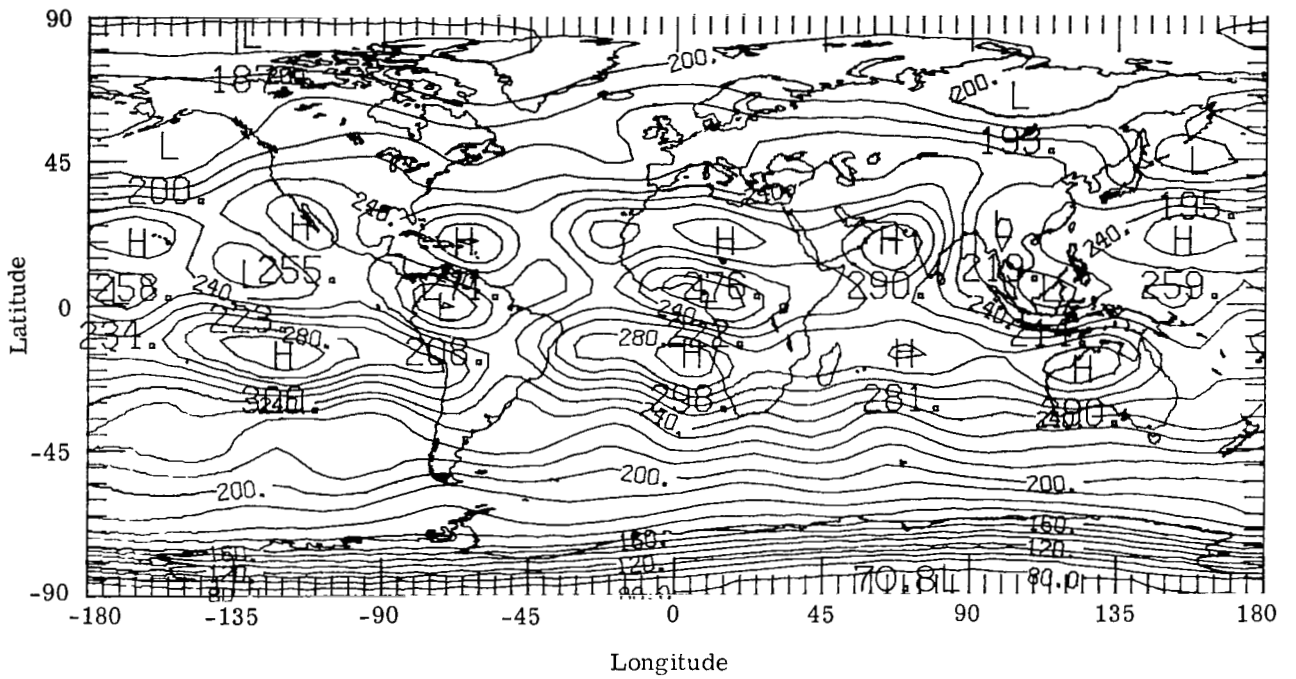


(i) March 1976.

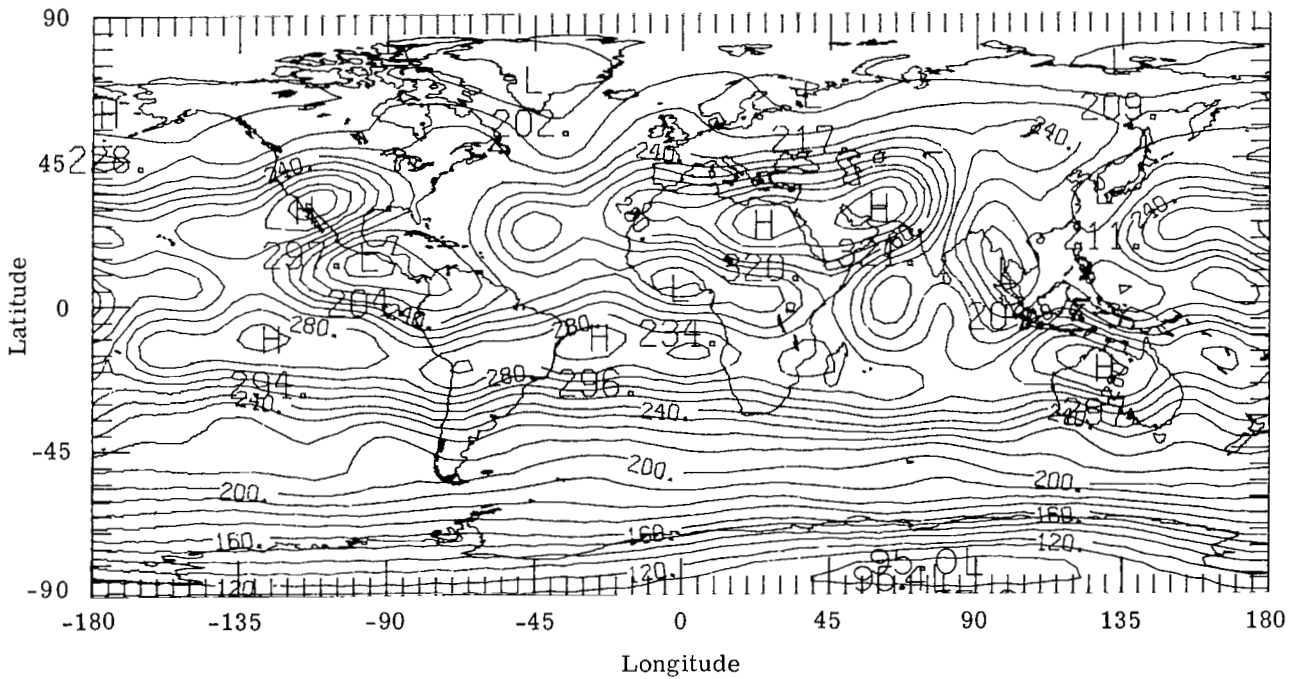


(j) April 1976.

Figure 8.- Continued.



(k) May 1976.



(l) June 1976.

Figure 8.- Concluded.

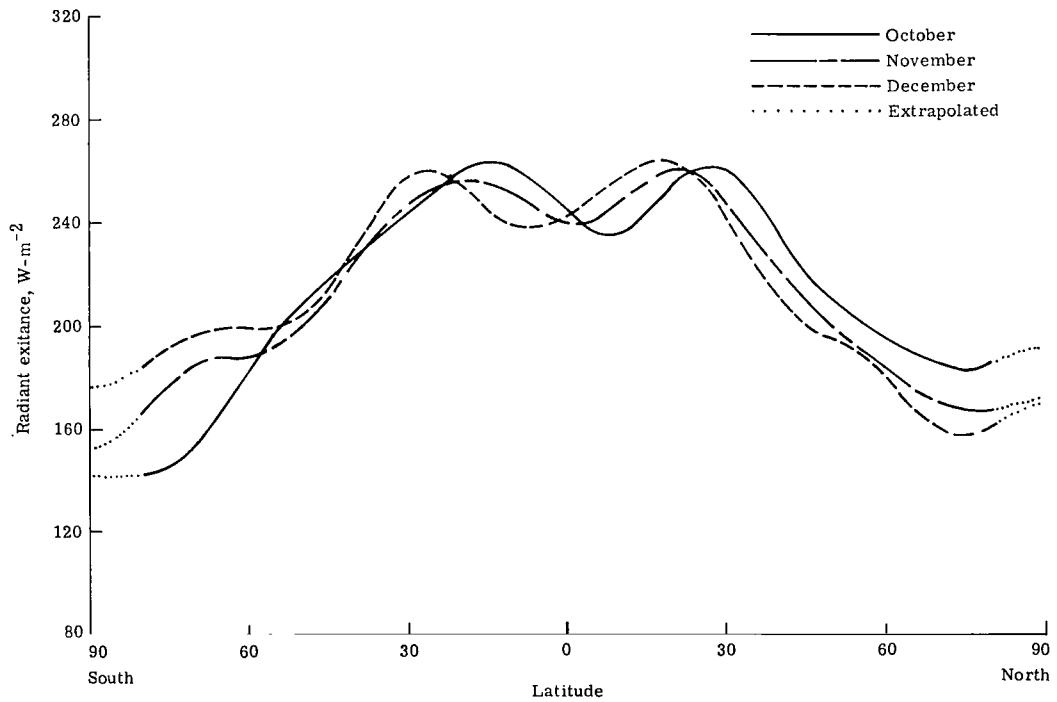
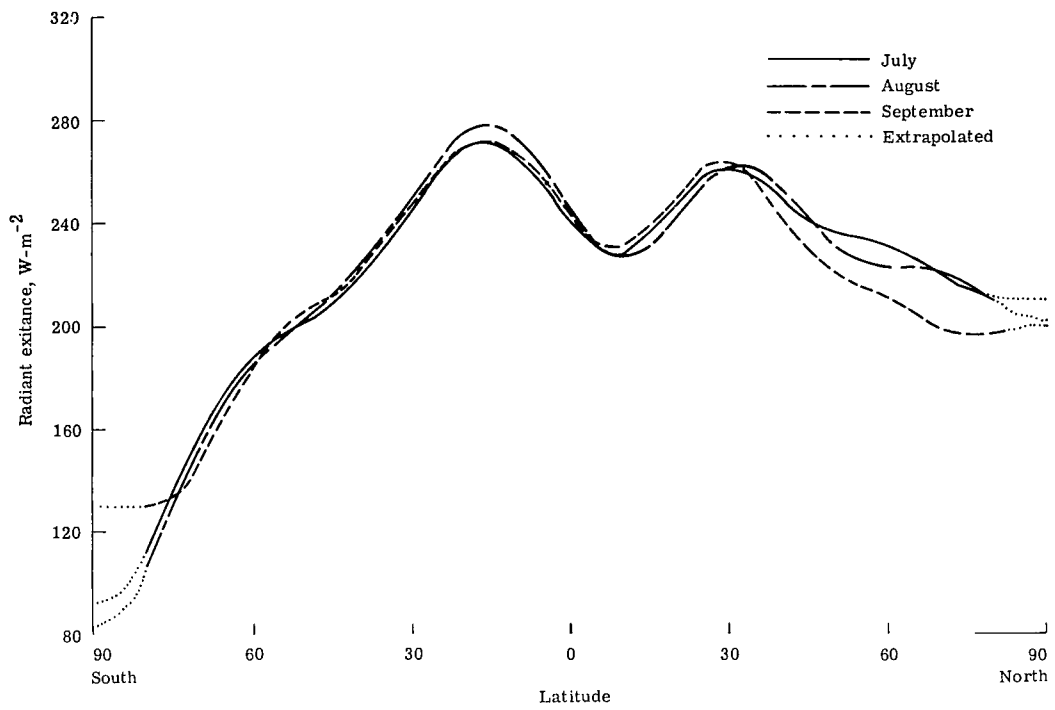


Figure 9.- Monthly averages of zonal emitted radiant exitance ($W\cdot m^{-2}$).

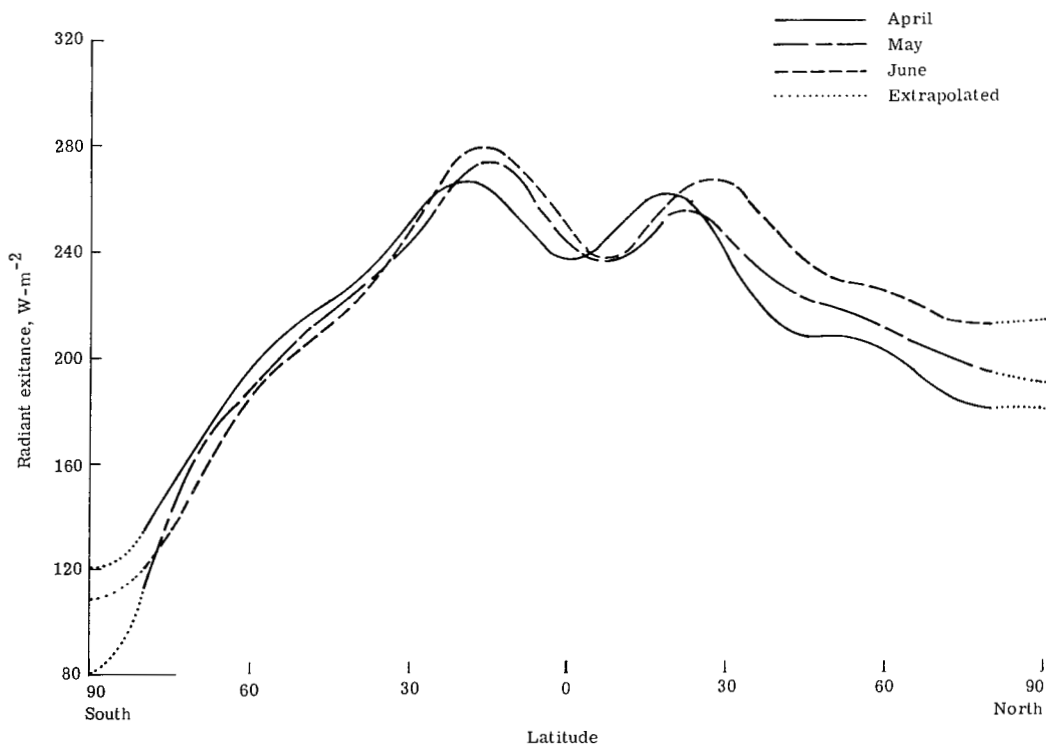
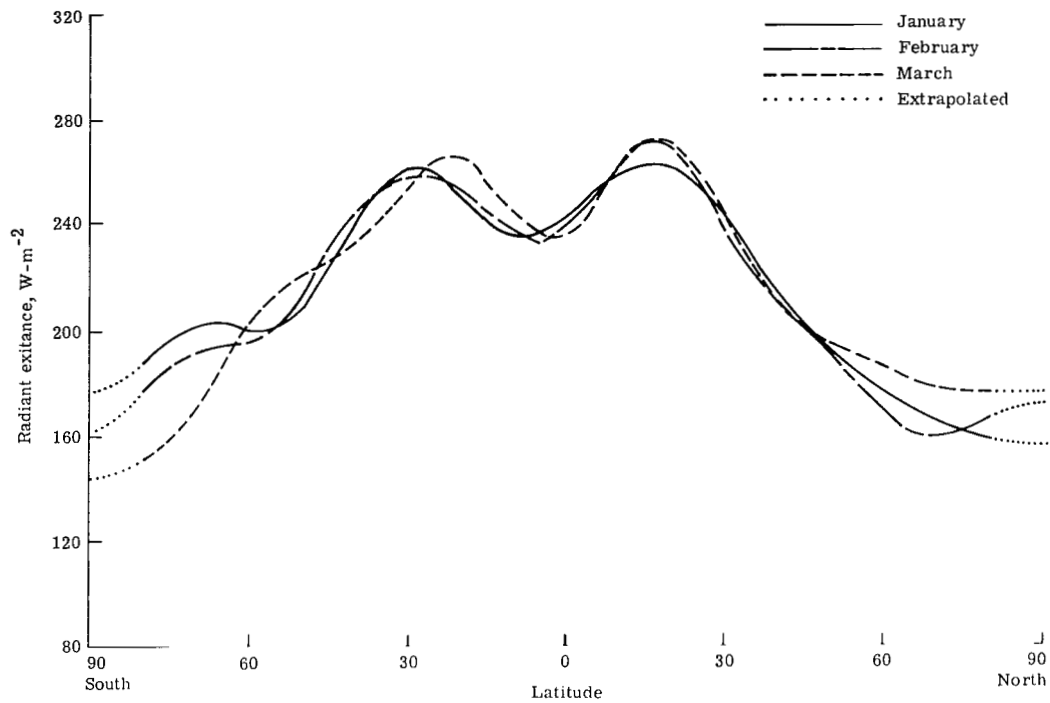


Figure 9.- Concluded.

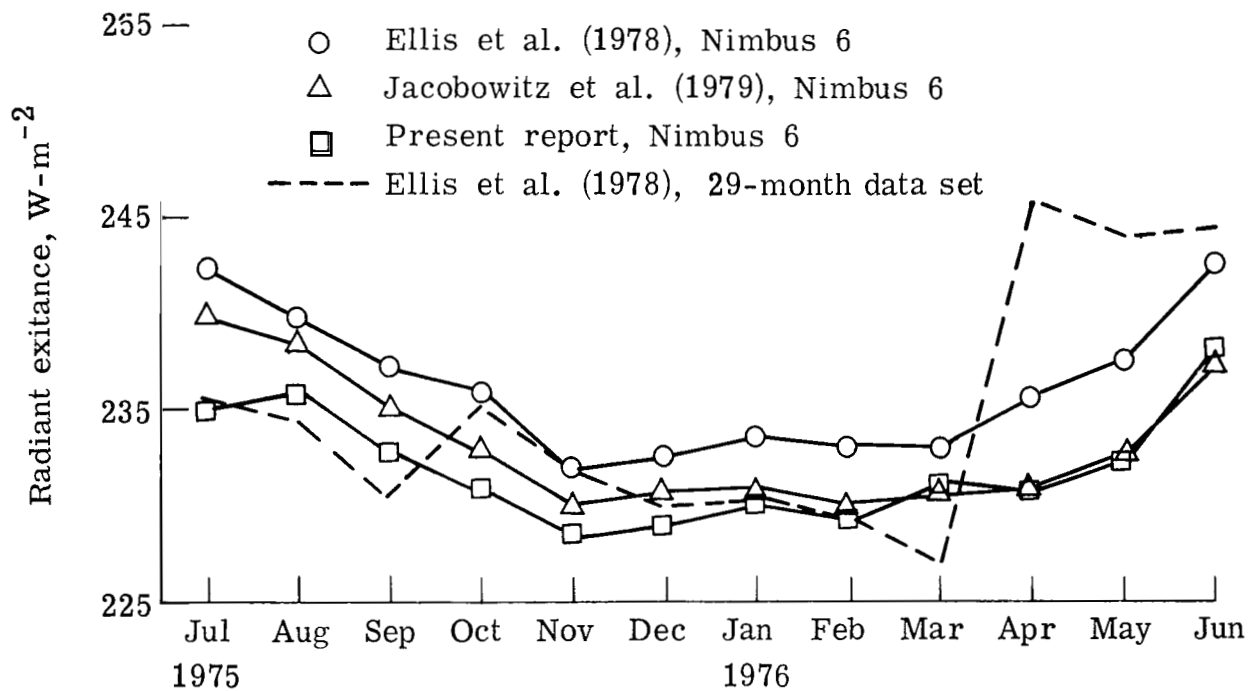


Figure 10.- Time histories of global mean from Nimbus 6 wide-angle radiometer for July 1975 through June 1976 (29-month composite data set for 1964 through 1971 represented by dashed line).

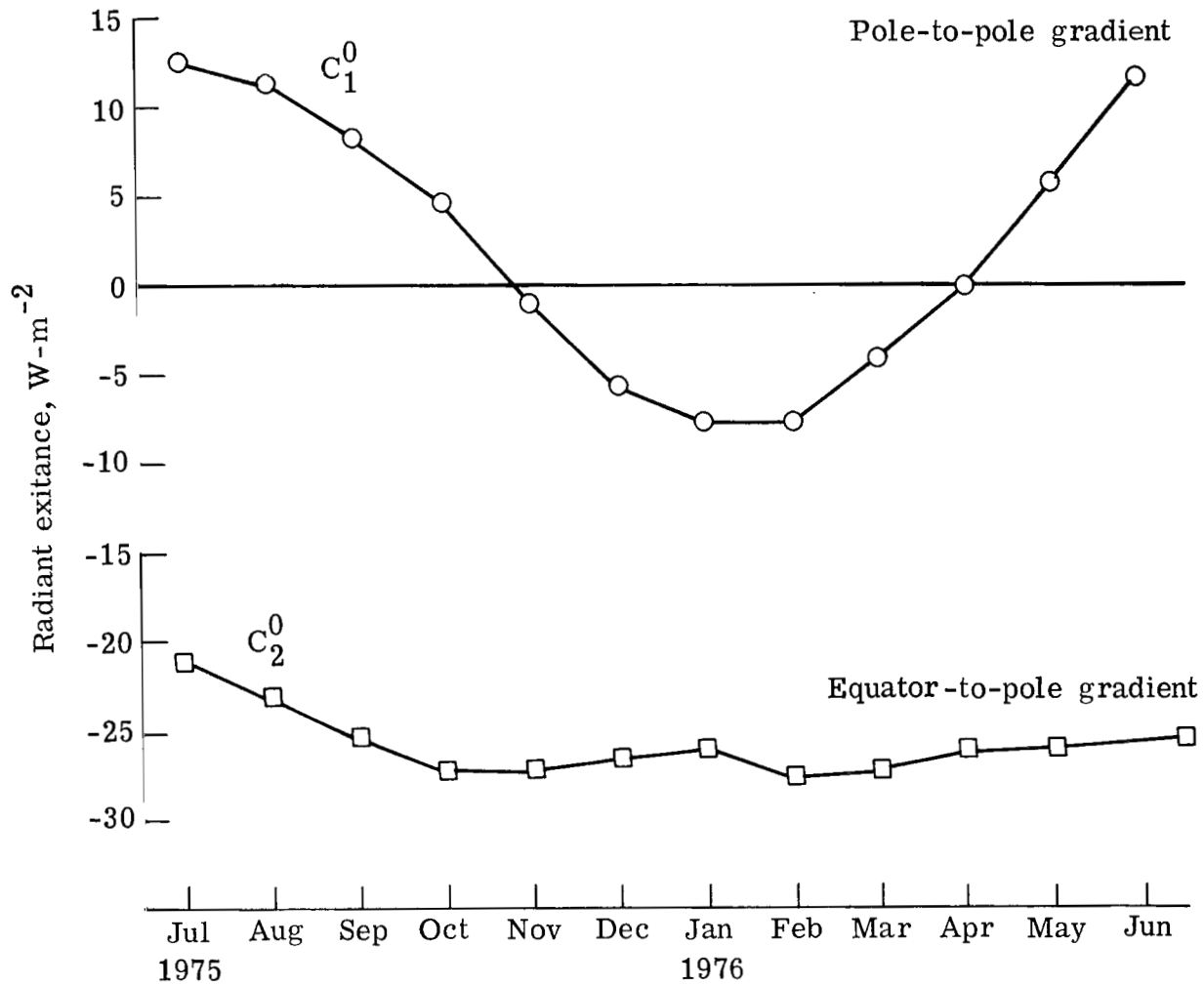


Figure 11.- Time histories of pole-to-pole gradient C_1^0 and equator-to-pole gradient C_2^0 for July 1975 through June 1976.

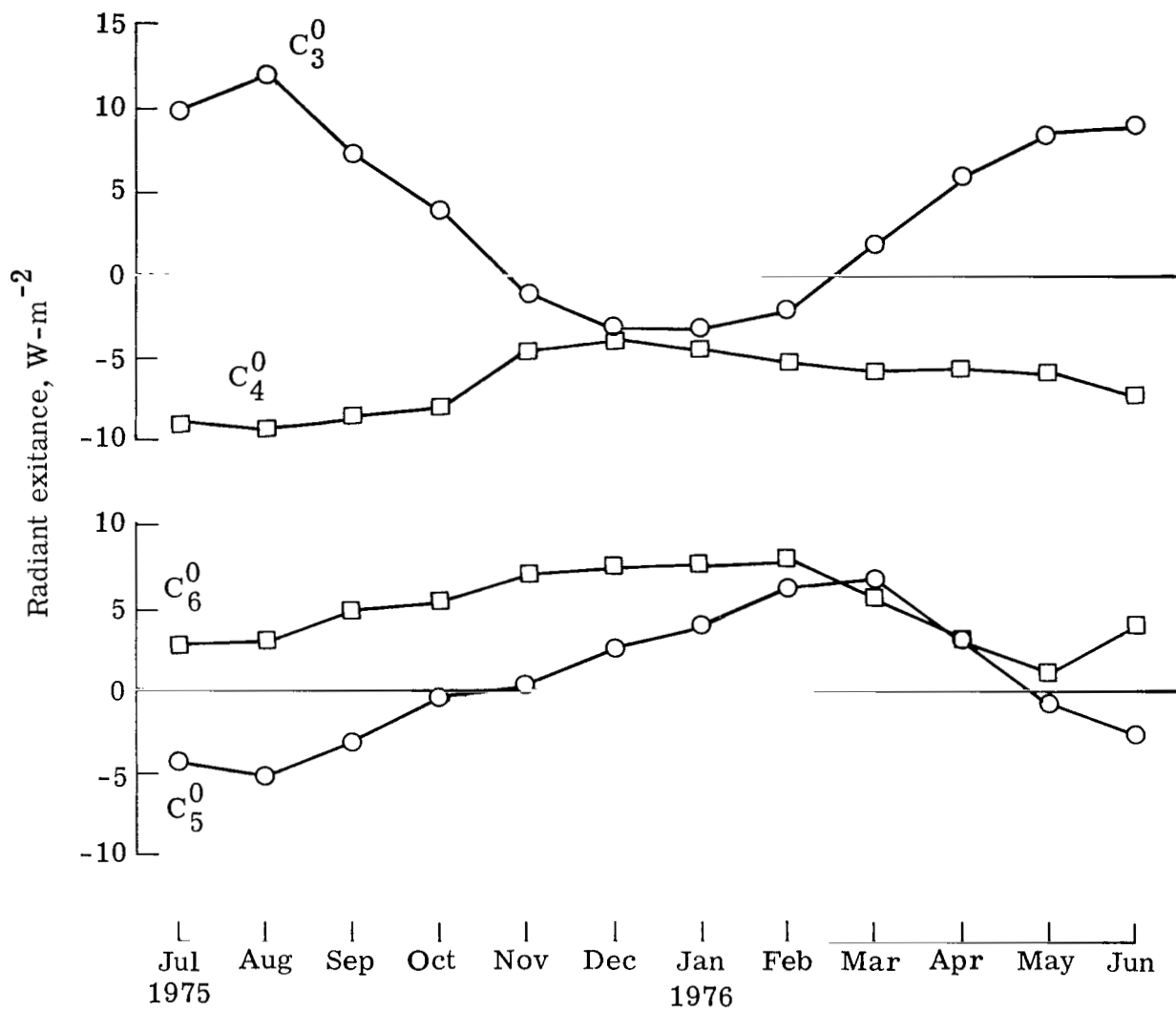


Figure 12.- Time histories of C_n^0 for $n = 3$ to $n = 12$ for July 1975 through June 1976.

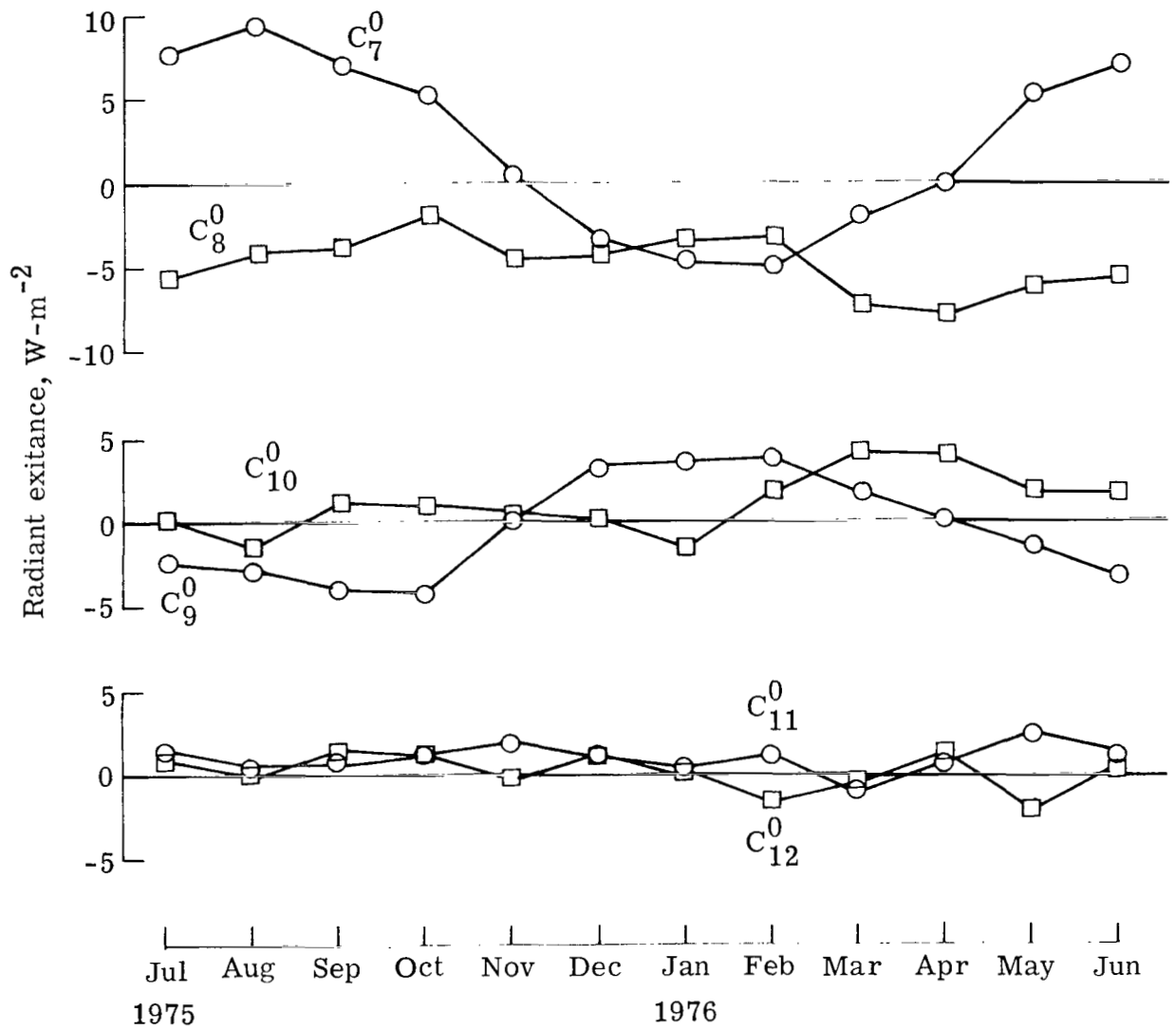


Figure 12.- Concluded.

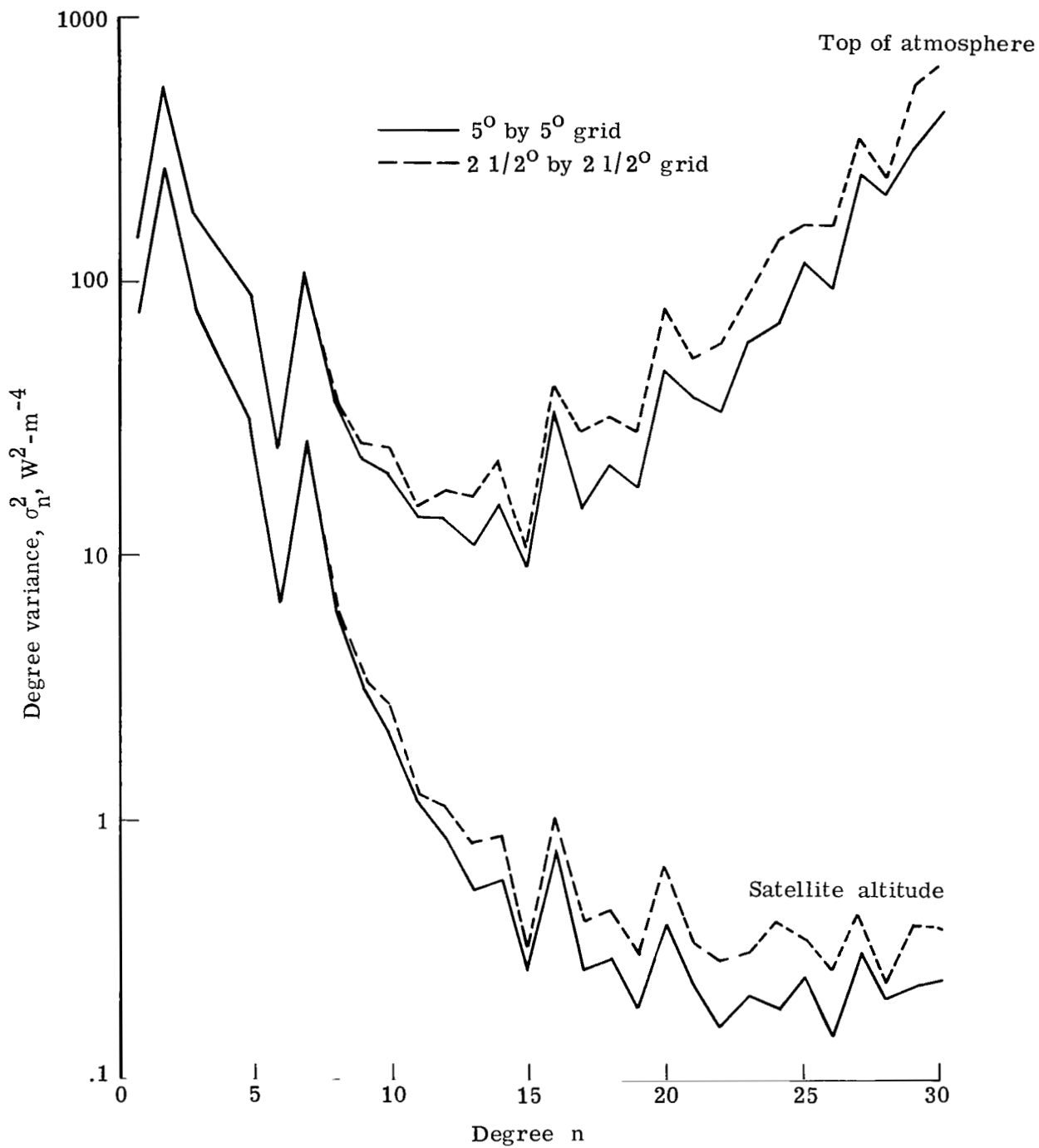


Figure 13.- Comparison of degree variance plots for August 1975 for 5° and $2\frac{1}{2}^\circ$ grid systems.

1. Report No. NASA TP-1746		2. Government Accession No.		3. Recipient's Catalog No.	
4. Title and Subtitle DECONVOLUTION AND ANALYSIS OF WIDE-ANGLE LONGWAVE RADIATION DATA FROM NIMBUS 6 EARTH RADIATION BUDGET EXPERIMENT FOR THE FIRST YEAR				5. Report Date December 1980	
7. Author(s) T. Dale Bess, Richard N. Green, and G. Louis Smith				6. Performing Organization Code 146-10-06-02	
9. Performing Organization Name and Address NASA Langley Research Center Hampton, VA 23665				8. Performing Organization Report No. L-13873	
12. Sponsoring Agency Name and Address National Aeronautics and Space Administration Washington, DC 20546				10. Work Unit No.	
15. Supplementary Notes				11. Contract or Grant No.	
16. Abstract One year of longwave radiation data from July 1975 through June 1976 from the Nimbus 6 satellite Earth radiation budget experiment is analyzed by representing the radiation field by a spherical harmonic expansion. The data are from the wide-field-of-view instrument. Contour maps of the longwave radiation field and spherical harmonic coefficients to degree 12 and order 12 are presented for a 12-month data period.				13. Type of Report and Period Covered Technical Paper	
17. Key Words (Suggested by Author(s)) Earth radiation budget Longwave radiation Nimbus 6 Data analysis Deconvolution Spherical harmonics				14. Sponsoring Agency Code	
18. Distribution Statement Unclassified - Unlimited				15. Supplementary Notes	
19. Security Classif. (of this report) Unclassified		20. Security Classif. (of this page) Unclassified		21. No. of Pages 59	
				22. Price A04	
				Subject Category 47	

National Aeronautics and
Space Administration

Washington, D.C.
20546

Official Business

Penalty for Private Use, \$300

THIRD-CLASS BULK RATE

Postage and Fees Paid
National Aeronautics and
Space Administration
NASA-451



9 1 1U, E, 120580 S00903DS
DEPT OF THE AIR FORCE
AF WEAPONS LABORATORY
ATTN: TECHNICAL LIBRARY (SUL)
KIRTLAND AFB NM 87117

NASA

POSTMASTER: If Undeliverable (Section 158
Postal Manual) Do Not Return
